AUT Journal of Electrical Engineering
10.22060/EEJ.2025.24278.5667

From DC to Holistic Centrality: AI-Driven Estimation for Enhanced Power Network Analysis

Mohammad Shahraeini*[1], Masoud Besharatloo[2]

[1]Assistant Professor, Department of Electrical Engineering, Golestan University, Gorgan, Iran (m.shahr@gu.ac.ir)
[2]Master's Graduate, Faculty of Engineering, Golestan University, Gorgan, Iran

Abstract:

This paper introduces a novel approach to power system analysis by integrating *DC Holistic Centrality* with advanced deep learning (DL) techniques to enhance the efficiency and accuracy of grid operation assessments. We propose DC Holistic Centrality, a computationally efficient measure derived from DC load flow data, which extends traditional operational centrality by incorporating generation and demand nodes as pendant buses. Leveraging this new metric, we develop a suite of AI-driven estimation methods: a linear regression baseline for active holistic betweenness prediction, a deep neural network (DNN) for accurate cross-bus prediction of active holistic betweenness, a convolutional neural network (CNN) for voltage magnitude estimation from DC holistic dependency matrices, and a scalability assessment using the IEEE 57-bus system to validate model robustness. The study utilizes a comprehensive dataset generated from varied operational scenarios, with feature selection guided by correlation analyses rather than additional extraction techniques. Results demonstrate significant improvements in capturing inter-bus dependencies and system dynamics, offering a promising framework for real-time grid monitoring and management.

Keywords: Complex Power Networks, DC Holistic Centrality, Deep Learning, Cross-bus Prediction, Voltage Magnitude Estimations.

1. Introduction

The analysis of power systems as complex networks, known as *Complex Power Networks*, has received considerable attention in electrical engineering. This concept, introduced by Barabási *et al.*, characterized the power grid as a scale-free network, transforming the understanding of power grid structures. This viewpoint has provided valuable insights into the interconnected nature of power systems, influencing their operation, evaluation, vulnerability, reliability, and resilience [1-3].

The study of complex networks and the use of metrics to assess their properties are now crucial in many fields, including electrical engineering. Metrics such as clustering, distance, centrality, and scaling are utilized to measure and classify these networks. Centrality metrics are primarily categorized into neighborhood-based (e.g., Eigen centrality and degree centrality) and shortest path-based measures (e.g., betweenness [4] and closeness [5]).

1-1- Centrality Metrics in Complex Power Graphs

The exploration of centrality metrics in complex power networks has evolved significantly since the early 21st century, offering critical insights into the structural and operational dynamics of power systems. These metrics, which quantify the importance of nodes (buses) and edges (transmission lines) within a network, are broadly classified into two categories: neighborhood-based and shortest path-based measures. Neighborhood-based metrics, such as degree centrality and eigenvector centrality, assess a node's influence based on its direct connections or the significance of its neighbors. In contrast, shortest path-based metrics, including betweenness and closeness centrality, evaluate a node’s role in facilitating power flow along the network's most efficient paths [6].

In power systems, centrality metrics have been adapted to reflect electrical properties, giving rise to structural and operational variants. Structural centrality incorporates electrical distances (derived from line impedances) as edge weights, making it sensitive to changes in grid topology [7]. Our prior work [6] demonstrated that structural centralities diverge from traditional graph-based measures by emphasizing

these electrical distances, providing a more nuanced view of network connectivity. Operational centrality, however, integrates power flow capacities and system states (e.g., voltage magnitudes and phase angles), either directly or indirectly, using data from AC or DC load flow analyses [8, 9]. This category encompasses diverse forms, accounting for active and reactive power flows, which are essential for capturing the dynamic behavior of electrical grids.

Our previous studies [1, 6, 10] have extensively analyzed these centrality types. In [6], we highlighted how structural centralities differ from graph-based ones by leveraging electrical distances, while operational centralities incorporate power flow magnitudes for deeper system insights. In [10], we compared AC and DC power flow impacts, revealing that DC approximations, despite minor errors, reliably preserve key trends, making them suitable for large-scale or real-time applications. Building on this, [1] introduced "*Holistic Electrical Centrality*", a novel operational centrality that models generations and demands as pendant nodes. This approach addresses interpretability limitations in traditional operational betweenness metrics, showing stronger correlations with voltage magnitudes and reactive power flows, thus reinforcing the value of a holistic system perspective.

These centrality measures (i.e., structural, operational, and even new holistic one) play a pivotal role in power system analysis, enhancing understanding of grid structure and operational dynamics [7-11]. They have informed the design of resilient grid architectures [11-15], optimized operational strategies [16], and supported resource allocation tasks, such as phasor measurement unit (PMU) placement [17-20], microgrid and renewable source positioning [6, 21-25], and wide area measurement system (WAMS) design [26, 27]. Additionally, they have been instrumental in vulnerability assessments, critical node identification, and reliability enhancements [6], underscoring their versatility in addressing modern power system challenges.

1-2- AI-Driven Power Flow Analysis

Power flow analysis is a fundamental computational technique used to evaluate and establish the steady-state operating conditions of electrical power systems by calculating the voltage magnitudes and phase angles at each bus. This analysis is essential for ensuring the reliability, stability, and optimal functioning of power systems [28-32]. While the application of deep learning (DL) algorithms in power flow analysis is not a recent innovation [28, 29], recent advancements have significantly expanded its role in enhancing the accuracy and scalability of these analyses [30, 32-34].

Adaptive and physically informed deep neural networks, such as PINN4PF, have emerged as powerful tools, effectively captured network topology and improved power flow predictions across large-scale grids [30]. These developments reflect a growing trend toward integrating domain-specific knowledge into DL frameworks. Recent research has explored a variety of deep neural architectures to address the complexities of modern power systems. Radial basis function networks, multi-layer perceptrons, and convolutional neural networks (CNNs) have been successfully applied to handle unbalanced and data-rich distribution systems, delivering high accuracy and robustness [32]. Furthermore, advancements in graph deep learning have enhanced the management of non-Euclidean data and dynamic conditions, supporting reliable and efficient power flow analysis in networks integrated with renewables [33]. This evolution underscores the versatility of DL in adapting to the evolving demands of power grids. Beyond power flow analysis, deep learning has demonstrated broader utility in power system applications. For instance, [34] proposed an enhanced fault detection and classification method for AC microgrids by combining data processing techniques with deep neural networks, highlighting its adaptability.

In the context of operational centrality, a recent innovation involves using these measures as input features for DL models. Our previous work [10] utilized DC betweenness measures (derived from DC load flow analysis) as inputs to a deep neural network to estimate total active power loss, demonstrating their effectiveness in capturing grid dynamics. This approach lays the groundwork for the current study, which leverages AI to refine centrality-based estimations, further bridging traditional engineering methods with advanced computational techniques.

1-3- Research Gap and Research Motivation

The integration of operational centrality measures and deep learning algorithms in power system analysis represents an emerging yet underexplored domain, revealing significant research gaps that this study seeks to address. While operational centrality, particularly the recently introduced holistic electrical centrality [1], has shown promise in capturing power system dynamics, its application remains limited by the computational complexity of traditional AC load flow-based calculations and the need for more comprehensive investigations across diverse energy flow types. Concurrently, the use of DL for power flow analysis has gained traction [10, 28-30, 32-34], yet prior efforts, such as those estimating total active power loss using DC betweenness measures [10], suffer from suboptimal accuracy and a narrow focus on specific neural architectures, notably excluding convolutional neural networks (CNNs). This study identifies a critical gap in leveraging holistic centrality measures with advanced DL techniques to enhance efficiency and accuracy, particularly for estimating key system parameters like active holistic betweenness and voltage magnitudes, which are essential for modern grid management but challenging to derive from simplified DC models.

The motivation for this research is to firstly introduce DC Holistic Centrality as a novel measure and then, explore its potential as input features for various DL methods, including linear regression, deep neural networks (DNNs), and convolutional neural networks. Additionally, we aim to assess the stability of these DL models in predicting critical power system parameters, addressing the need for efficient and reliable grid analysis tools.

1-4- Research Contributions

The contributions of this work are as follows:

- This study extends the concept of holistic centrality by introducing "*DC Holistic Centrality*", leveraging DC load flow information to provide a computationally efficient alternative for evaluating active power flow dynamics within power networks.

- We propose a linear regression model to establish a baseline for estimating active holistic betweenness from DC holistic measures, offering a simple yet effective approach to validate the feasibility of DL-based predictions.
- We then develop a deep neural network (DNN) to perform cross-bus prediction of active holistic betweenness of some buses using DC holistic inputs from other buses, demonstrating improved accuracy in capturing inter-bus dependencies.
- We explore a convolutional neural network (CNN) to estimate voltage magnitudes from DC holistic dependency matrices, demonstrating the potential and limitations of CNNs in capturing non-linear grid characteristics.
- We assess the scalability of the proposed DL approaches, validating their robustness and adaptability across the larger system, thus supporting their applicability to complex power networks.

1-3- Paper Structure

The remainder of this paper is organized as follows: Section 2 outlines the fundamentals of power network analysis, including load flow methods and graph representations. Section 3 introduces DC holistic centrality as a novel measure. Section 4 evaluates its performance through simulations, specifically their correlations with system states. Section 5 details AI-enhanced estimation techniques, covering data preparation (5-1), baseline and DNN estimation (5-2), cross-bus prediction (5-3), CNN-based voltage estimation (5-4), and scalability on the IEEE 57-bus system (5-5). The paper concludes with a summary of findings and future directions.

2. Preliminaries on Complex Power Network Analysis

This section provides the foundational concepts necessary for understanding the analysis of complex power networks as applied in this study. It introduces load flow analysis as a key method for assessing steady-state conditions, followed by the representation of power systems as graphs, including the novel holistic power graph. These preliminaries establish the theoretical framework for deriving centrality

10.22060/EEJ.2025.24278.5667

measures and integrating them with AI-driven techniques, setting the stage for the subsequent sections on holistic centrality and estimation methods.

2-1- Load Flow Analysis

Power flow analysis is a cornerstone of electrical engineering, essential for determining the steady-state operating conditions of power systems by calculating voltage magnitudes and phase angles at all buses. This process is critical for ensuring system reliability, stability, and optimal performance under varying operational scenarios [28-30]. Two primary methods are employed: AC load flow, which provides a comprehensive analysis by accounting for both active and reactive power flows with detailed voltage considerations, and DC load flow, a simplified approximation focusing solely on active power using linear assumptions. These methods cater to different needs, with AC offering precision for detailed studies and DC enabling efficient computations for large-scale or real-time applications, both of which are leveraged in this study to support centrality and AI-based analyses [10].

2-1-1- AC Load Flow

The analysis of AC power flow is indispensable for a thorough understanding of power dynamics within electrical networks. It considers both active power (P), measured in watts (W), which represents the usable energy delivered to loads, and reactive power (Q), measured in volt-amperes reactive (VAR), which accounts for the energy stored and released by inductive and capacitive elements. These power components are governed by complex power equations derived from Kirchhoff's laws, expressed as $S=P+\mathrm{j}Q$, where S is the complex power in volt-amperes (VA). The power flow at bus i, S_i , is related to the voltage V_i at that bus and the admittances of connected lines, formulated as:

$$\begin{aligned} S_i &= P_i + jQ_i = V_i \sum_{j=1}^{n} Y_{ij} V_j^* \\ P_i &= \sum_{j=1}^{n} |V_i||V_j| \left(Y_{ij}\cos(\theta_{ij})\right) \\ Q_i &= \sum_{j=1}^{n} |V_i||V_j| \left(Y_{ij}\sin(\theta_{ij})\right) \end{aligned} \tag{1}$$

10.22060/EEJ.2025.24278.5667

where P_i and Q_i are the active and reactive power at bus i, $|V_i|$ and $|V_j|$ are the voltage magnitudes, Y_{ij} is the admittance between buses i and j, and θ_{ij} is the phase angle difference.

This non-linear system requires iterative numerical methods, such as the Newton-Raphson or Gauss-Seidel techniques, to solve for steady-state voltages, offering detailed insights into power consumption, generation, and losses across the grid [31].

2-1-2- DC Load Flow

DC power flow analysis offers a streamlined approach by focusing exclusively on active power (P) flow, simplifying the computational burden for large power systems. It assumes constant voltage magnitudes (typically 1 per unit) and approximates small phase angle differences with $\sin(\theta) \approx \theta$. The power flow equation is expressed as [31]:

$$P_i = \sum_{j=1}^{n} B_{ij} \left(V_i - V_j \right) \tag{2}$$

where P_i is the active power injected at bus i, and B_{ij} is the susceptance between buses i and j. In matrix form, this becomes $P=B.\theta$, enabling efficient calculations. The power flow P_{ij} from bus i to j is proportional to the voltage angle difference:

$$P_{ij} = B_{ij} \left(\theta_i - \theta_j \right) \tag{3}$$

This model is widely adopted for operational planning and real-time monitoring due to its simplicity and speed, making it a practical choice for deriving approximate centrality measures in this study.

2-2- Power Graph

The power graph is a simple undirected graph that represents the power grid, where vertices (V) symbolize system buses and edges (E) correspond to transmission lines. This graph can be either unweighted or weighted, with weights reflecting electrical distances based on the absolute values of line impedances ($|Z_{ij}|$). Thus, the weighted power graph is denoted as $G_Z(V,E,w)$ [20], where V represents the set of buses, E the set of transmission lines, and w the weight function. This representation facilitates the

10.22060/EEJ.2025.24278.5667

application of graph theory to analyze network topology and connectivity, providing a foundation for centrality calculations.

2-3- Holistic Power Graph

The holistic power graph, first introduced in [1], offers a novel framework for calculating credible centrality values, particularly betweenness, by including all electric buses, even those not directly involved in electrical shortest paths. This approach addresses limitations in traditional operational centrality methods, which focused primarily on power flows through transmission lines and bus inflow/outflow without considering bus types. By modeling generators and demands as separate pendant nodes, the holistic graph provides a comprehensive structure: generator nodes inject power, and demand nodes receive it. However, determining the electrical distances for these pendant nodes poses challenges, especially for demand nodes, though their betweenness is set to zero, minimizing distance-related concerns for this metric. Depending on the energy flow type, the holistic graph is classified as active or reactive. Steps 2 to 10 of Algorithm 1 detail the derivation of the holistic graph from DC load flow results, termed the DC holistic graph, while reactive flows generate the reactive holistic graph. Figs. 2 and 3 illustrate the active and reactive holistic graphs for the IEEE 14-bus test case, with red pendants representing generation nodes and green pendants denoting demand nodes.

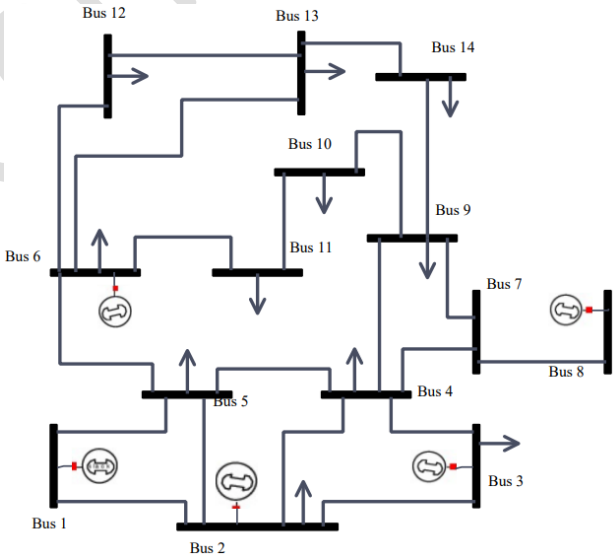

Fig. 1. IEEE 14-bus test system, considering all generations and demands [6].

10.22060/EEJ.2025.24278.5667

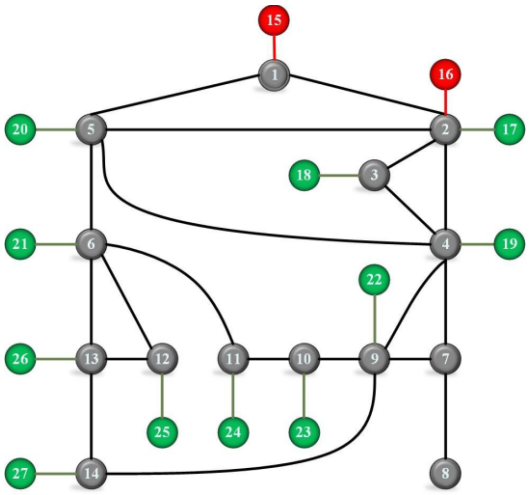

Fig. 2. Active Holistic Graph: Adding Active Generations and Demands as the Pendants to IEEE 14-Bus Network

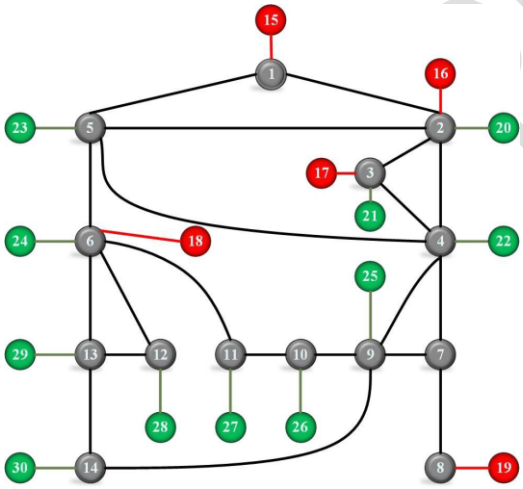

Fig. 3. Reactive Holistic Graph: Adding Reactive Generations and Demands as the Pendants to IEEE 14-Bus Network

3. Holistic Electrical Centrality Measures

This section introduces and analyzes holistic electrical centrality, an extension of traditional operational centrality tailored for power networks. Unlike conventional approaches that overlook the distinct roles of generation and demand nodes, holistic centrality incorporates them explicitly as pendant nodes, offering a more realistic view of power flow dynamics. We begin by constructing the holistic power graph (described in section 2-3) and defining the associated dependency matrix, which quantifies how strongly each bus relies on others to transmit power along the network's electrical shortest paths. These formulations serve as the foundation for the AI-based estimations discussed later in the paper.

3-1-Bus Dependency Matrix

10.22060/EEJ.2025.24278.5667

Operational centrality measure is based on electrical distances and also flow information of edges in the power graph, either the original one (G_Z) or holistic one ($\overset{H}{G}_Z$) [1].

Recall that the power graph is denoted as G_Z (resp. holistic graph as $\overset{H}{G}_Z$). Let f_{st} represent the maximum power flowing along the shortest electrical path between buses s and t, while $f_{st}(k)$ indicates the maximum inflow or outflow at bus k within that same path. The dependency between pairs of buses describes the extent to which bus s relies on bus k to effectively distribute its power flow along the shortest electrical path to all other buses t in the power grid. In a system comprising n buses (resp. $n+n_G+n_D$ in holistic graph; where n_G and n_D are numbers of generation and demands), this dependency of bus s on bus k for transmitting power to the other buses can be represented as follows:

$$d_{sk} = \sum_{\substack{t=1 \\ s\neq t\neq k\in V}}^{n} \frac{f_{st}(k)}{f_{st}} \tag{4}$$

It is important to note that f_{st} and $f_{st}(k)$ can represent either active or reactive power flows, depending on the context. Both active and reactive values can be derived from AC load flow analysis, or it can specifically indicate active power flows when calculated using DC load flow analysis [10].

The dependency of bus pairs within the entire system can be presented matrix **D** as follows [9, 10]:

$$\mathbf{D} = \begin{bmatrix} d_{11} & d_{12} & \cdots & d_{1n} \\ d_{21} & d_{22} & \cdots & d_{2n} \\ \vdots & \vdots & \ddots & \vdots \\ d_{n1} & d_{n2} & \cdots & d_{nn} \end{bmatrix} \tag{5}$$

Every entry in the matrix **D** represents the extent to which a bus, identified by its row number, relies on another bus, identified by its column number, to efficiently transfer power along the shortest electrical path to all other buses in the system. This matrix underscores the importance of each bus as a junction within the network for the transmission of power (whether active or reactive), which is why it is referred to as the "*Dependency Matrix*" [6].

10.22060/EEJ.2025.24278.5667

Different variations of **D** matrices derived from AC/DC flows, including: the active dependency matrix ($\mathbf{D}_p$), DC dependency matrix ($\mathbf{D}_{dc}$), and holistic DC dependency matrix ($\overset{H}{\mathbf{D}}_{dc}$), are presented for the normal operational conditions of the IEEE 14-bus system (illustrated in Fig. 1) in the Figs. 4 to 6. These matrices are normalized to a scale between 0 and 1. To enhance visualization, a color gradient is employed: values close to 1 are represented in red, while those near 0 are shown in white, with a smooth transition of red shades between these extremes. The process for constructing the DC holistic dependency matrix ($\overset{H}{\mathbf{D}}_{dc}$) from the results of the DC load flow analysis is detailed in Algorithm 1.

The analysis of the active dependency matrix and the DC dependency matrix, as illustrated in Figs. 4 and 5, reveals notable similarities between the two. Both matrices are based on active flows within the grid; however, the active dependency matrix is derived from precise values obtained through AC load flow calculations, while the DC dependency matrix relies on less accurate results from DC flow analysis. It can also be observed that certain nodes do not participate in any shortest paths, resulting in corresponding columns with zero values (e.g., nodes 1, 2, 12, and 14 in the active and DC dependency matrices). Moreover, pendant nodes, which also do not contribute to the shortest paths, exhibit zero values in their respective columns (e.g., node 8 in the active and DC dependency matrices and nodes 15 to 27 in the holistic DC dependency matrix). These zero-value columns lead to zero betweenness centrality for the associated nodes. It is noteworthy that the main diagonal of each dependency matrix is composed entirely of zeros, reflecting the absence of any dependency between a node and itself.

In conclusion, the dependency matrix of a grid can be interpreted as a 2-D image representing the dynamics of the grid under the specified operational conditions, i.e., its energy flows. This matrix also encapsulates structural information, including the shortest paths within the grid. These 2-D images serve as effective inputs for various neural network architectures, particularly convolutional neural networks (CNNs). In this context, we will present an application that leverages these 2-D images within an AI-driven estimator.

Algorithm 1 Calculating DC Holistic Dependency Matrix

Inputs: `mpc` structure; including electrical grid structure and generations/demands for load flow

Output: DC holistic dependency matrix

Procedure $\overset{H}{\mathrm{D}}_{dc}$ = `make_hol_dep(mpc)`

Initialize: Extract matrix Y_{bus}=`makeYbus(mpc)`; Active generations p_{Gi}; Active demands P_{Dj} from `mpc` structure

Represent the power grid as a weighted graph $G_Z(V, E, w)$ with $w_{ij} = |1/Y_{ij}|$;

Extract number of buses (n); Number of active generation (n_G); number of active loads (n_D)

Solve the DC load flow `LF_DC(mpc)`; to determine the flow in different lines of the system, represented by p_{ij};

$\overset{H}{G}_Z \leftarrow G_Z(V, E, w)$

For k=1 to n_G

For active generation in node k with generation p_{Gk}, add new node h as pendants connecting to k, with the flow of p_{hk}=p_{Gk} from h to k. The weight of new edge equal to 1 (w_{hk}=1).

$\overset{H}{G}_Z \leftarrow \overset{H}{G}_Z(V^{+k}, E^{+k}, w^{+1})$

End for

For q=1 to n_D

For active demand in node q with demand of p_{Dq}, add new node r as pendants connecting to q, with the flow of p_{qr}=p_{Dq} from q to r. The weight of new edge equal to 1 (w_{qr}=1).

$\overset{H}{G}_Z \leftarrow \overset{H}{G}_Z(V^{+q}, E^{+q}, w^{+1})$

End for

Determine the collection of electrical shortest paths for the weighted graph $\overset{H}{G}_Z$;

Having all p_{ij} from DC load flow, p_{hk}, and p_{qr} from step (5-10), then calculate the maximum power transmission p_{st} along the shortest electrical path between buses s and t. Identify $p_{st}(k)$, which represents the highest inflow or outflow at bus k along this path.

For s=1 to $n+n_G+n_D$

For k=1 to $n+n_G+n_D$

Calculate dependency of node s on node k (d_{sk}) in $\overset{H}{G}_Z$ based on calculate p_{st} and $p_{st}(k)$ in steps (12) and Eq. (4).

End for

End for

Return $\overset{H}{\mathrm{D}}_{dc}$

0	0.68	0	0.17	0.39	0.18	0.07	0	0.04	0	0	0	0	0
0	0	0	0.49	0.4	0.3	0.2	0	0.1	0	0	0	0	0
0	0.1	0	1	0.4	0.22	0.4	0	0.2	0	0	0	0	0
0	0.1	0	0	0.4	0.22	0.4	0	0.2	0	0	0	0	0
0	0	0	0.6	0	0.3	0.18	0	0.09	0	0	0	0	0
0	0	0	0.3	0.6	0	0.05	0	0	0.07	0.2	0	0.1	0
0	0.1	0	0.63	0.3	0.14	0	0	0.3	0.02	0	0	0	0
0	0.1	0	0.63	0.3	0.14	0.85	0	0.3	0.02	0	0	0	0
0	0.1	0	0.33	0	0.2	0.41	0	0	0.27	0.23	0	0	0
0	0.1	0	0.33	0	0.2	0.41	0	0.62	0	0.23	0	0	0
0	0	0	0.1	0.4	0.6	0.1	0	0.3	0.19	0	0	0	0
0	0	0	0.3	0.6	0.85	0.05	0	0	0.07	0.19	0	0.1	0
0	0	0	0.3	0.6	0.85	0.05	0	0	0.03	0.08	0	0	0
0	0.1	0	0.33	0	0	0.41	0	0.72	0.06	0	0	0.2	0

Fig. 4. Active Dependency Matrix (Dp) for normal operation condition of IEEE 14-bus system.

0	0.7	0	0.19	0.4	0.18	0.08	0	0.04	0	0	0	0	0
0	0	0	0.5	0.4	0.3	0.21	0	0.1	0	0	0	0	0
0	0.1	0	1	0.4	0.21	0.4	0	0.2	0	0	0	0	0
0	0.1	0	0	0.4	0.21	0.4	0	0.2	0	0	0	0	0
0	0	0	0.6	0	0.3	0.18	0	0.09	0	0	0	0	0
0	0	0	0.3	0.6	0	0.05	0	0	0.09	0.2	0	0.1	0
0	0.1	0	0.64	0.3	0.14	0	0	0.3	0.02	0	0	0	0
0	0.1	0	0.64	0.3	0.14	0.85	0	0.3	0.02	0	0	0	0
0	0.1	0	0.34	0	0.2	0.42	0	0	0.3	0.23	0	0	0
0	0.1	0	0.34	0	0.2	0.42	0	0.62	0	0.23	0	0	0
0	0	0	0.1	0.4	0.6	0.1	0	0.3	0.2	0	0	0	0
0	0	0	0.3	0.6	0.84	0.05	0	0	0.08	0.18	0	0.1	0
0	0	0	0.3	0.6	0.84	0.05	0	0	0.03	0.08	0	0	0
0	0.1	0	0.34	0	0	0.42	0	0.72	0.06	0	0	0.2	0

Fig. 5. DC Dependency Matrix (Ddc) for normal operation condition of IEEE 14-bus system.

0	0.56	0.02	0.13	0.36	0.16	0.05	0	0.04	0	0	0	0.01	0	0	0	0	0	0	0	0	0	0	0	0	0
0.04	0	0.04	0.36	0.36	0.28	0.14	0	0.1	0.01	0.01	0.01	0.02	0.01	0	0	0	0	0	0	0	0	0	0	0	0	0
0.04	0.15	0	0.76	0.36	0.2	0.28	0	0.2	0.01	0	0.01	0.01	0.02	0	0	0	0	0	0	0	0	0	0	0	0	0
0.04	0.15	0.04	0	0.36	0.2	0.28	0	0.2	0.01	0	0.01	0.01	0.02	0	0	0	0	0	0	0	0	0	0	0	0	0
0.04	0.08	0.04	0.43	0	0.28	0.13	0	0.09	0.01	0.01	0.01	0.02	0.01	0	0	0	0	0	0	0	0	0	0	0	0	0
0.04	0.08	0.04	0.19	0.44	0	0.02	0	0.04	0.08	0.16	0.04	0.12	0.03	0	0	0	0	0	0	0	0	0	0	0	0	0
0.04	0.15	0.04	0.56	0.28	0.14	0	0	0.28	0.03	0.01	0.01	0.01	0.02	0	0	0	0	0	0	0	0	0	0	0	0	0
0.04	0.15	0.04	0.56	0.28	0.14	0.65	0	0.28	0.03	0.01	0.01	0.01	0.02	0	0	0	0	0	0	0	0	0	0	0	0	0
0.04	0.15	0.04	0.32	0.04	0.2	0.26	0	0	0.24	0.2	0.04	0.04	0.04	0	0	0	0	0	0	0	0	0	0	0	0	0
0.04	0.15	0.04	0.32	0.04	0.2	0.26	0	0.41	0	0.21	0.04	0.04	0.04	0	0	0	0	0	0	0	0	0	0	0	0	0
0.04	0.08	0.04	0.11	0.36	0.54	0.04	0	0.19	0.14	0	0.04	0.04	0.04	0	0	0	0	0	0	0	0	0	0	0	0	0
0.04	0.08	0.04	0.19	0.44	0.64	0.02	0	0.04	0.07	0.16	0	0.1	0.04	0	0	0	0	0	0	0	0	0	0	0	0	0
0.04	0.08	0.04	0.19	0.44	0.66	0.02	0	0.04	0.04	0.08	0.04	0	0.04	0	0	0	0	0	0	0	0	0	0	0	0	0
0.04	0.15	0.04	0.32	0.04	0.04	0.26	0	0.5	0.08	0.02	0.04	0.2	0	0	0	0	0	0	0	0	0	0	0	0	0	0
1	0.38	0.02	0.09	0.12	0.05	0.03	0	0.02	0	0	0	0	0	0	0	0	0	0	0	0	0	0	0	0	0	0
0.04	0.96	0.04	0.36	0.36	0.28	0.14	0	0.1	0.01	0.01	0.01	0.02	0.01	0	0	0	0	0	0	0	0	0	0	0	0	0
0.04	0.96	0.04	0.36	0.36	0.28	0.14	0	0.1	0.01	0.01	0.01	0.02	0.01	0	0	0	0	0	0	0	0	0	0	0	0	0
0.04	0.13	0.96	0.38	0.24	0.13	0.08	0	0.06	0	0	0	0.01	0.01	0	0	0	0	0	0	0	0	0	0	0	0	0
0.04	0.15	0.04	0.92	0.36	0.2	0.16	0	0.12	0.01	0	0.01	0.01	0.01	0	0	0	0	0	0	0	0	0	0	0	0	0
0.04	0.08	0.04	0.43	0.96	0.28	0.13	0	0.09	0.01	0.01	0.01	0.02	0.01	0	0	0	0	0	0	0	0	0	0	0	0	0
0.04	0.08	0.04	0.19	0.44	0.85	0.02	0	0.04	0.06	0.12	0.03	0.12	0.03	0	0	0	0	0	0	0	0	0	0	0	0	0
0.04	0.15	0.04	0.31	0.04	0.08	0.26	0	0.79	0.07	0.06	0.01	0.02	0.02	0	0	0	0	0	0	0	0	0	0	0	0	0
0.04	0.15	0.04	0.32	0.04	0.19	0.26	0	0.41	0.48	0.17	0.03	0.04	0.04	0	0	0	0	0	0	0	0	0	0	0	0	0
0.04	0.08	0.04	0.11	0.36	0.54	0.04	0	0.19	0.14	0.36	0.04	0.04	0.04	0	0	0	0	0	0	0	0	0	0	0	0	0
0.04	0.08	0.04	0.19	0.44	0.64	0.02	0	0.04	0.07	0.16	0.46	0.09	0.04	0	0	0	0	0	0	0	0	0	0	0	0	0
0.04	0.08	0.04	0.19	0.44	0.66	0.02	0	0.04	0.04	0.08	0.02	0.62	0.04	0	0	0	0	0	0	0	0	0	0	0	0	0
0.04	0.15	0.04	0.32	0.04	0.04	0.26	0	0.45	0.05	0.01	0.02	0.15	0.61	0	0	0	0	0	0	0	0	0	0	0	0	0

Fig. 6. DC Holistic Dependency Matrix ($\mathbf{D}_{dc}^{H}$) for normal operation condition of IEEE 14-bus system.

Table 1 summarizes key quantitative features of the three dependency matrices illustrated in Figs. 4–6. While the active and DC matrices exhibit close alignment in terms of mean value and standard deviation, the holistic DC matrix differs with a larger matrix size (due to the addition of generation and demand

10.22060/EEJ.2025.24278.5667

pendants) and greater sparsity. Despite normalization, the holistic matrix shows reduced average dependency values, reflecting the distributed impact of added pendant nodes. This table supports the visual insights of Figs. 4–6 with a quantitative comparison that reinforces the validity of the DC-based approximation.

Table 1. Statistical Summary of Dependency Matrices

Metric	Active	DC	Holistic DC
Matrix size ($n \times n$)	14 × 14	14 × 14	27 × 27
Mean of nonzero entries	0.252	0.254	0.166
Standard deviation	0.230	0.232	0.181
Max value	1.00	1.00	1.00
Min (nonzero) value	0.02	0.02	0.01
Sparsity (% of zero entries)	56.12%	55.10%	63.17%

3-2-Operational Centrality Measures

As fully discussed in [1, 6], in a dependency matrix, the sum of the values in the *k*-th column of the dependency matrix indicates the operational betweenness centrality of the *k*-th bus within the analyzed power grid:

$$C_B^O(k) = \sum_{s=1}^{n} d_{sk} \tag{6}$$

Similarly, the inverse of the sum of the elements in the *s*-th row of the dependency matrix represents the operational closeness of the *s*-th bus in the system:

$$C_C^O(s) = \frac{1}{\sum_{k=1}^{n} d_{sk}} \tag{7}$$

The above operational centralities can be used besides of previously defined graph and structural centralities [6], i.e., C_B and C_B^S.

Table 2. Comparison of Different Electrical Betweenness Measures

	Graph Centrality	Structural Centrality	Operational Centrality		Holistic Centrality		
					AC Load Flow Analysis		DC Load Flow Analysis
					Active Flow	Reactive Flow	
Notation	C_B	C_B^S	C_B^P	C_B^Q	$\overset{H}{C}_B^P$	$\overset{H}{C}_B^Q$	$\overset{H}{C}_B^{dc}$
Network Structure	√	√	√	√	√	√	√
Electrical Distance	-	√	√	√	√	√	√
Load Flow Information	-	-	Active Flow	Reactive Flow	Active Flow	Reactive Flow	Active Flow
Generation/Demand Information	-	-	-	-	Active Gen/Dem	Reactive Gen/Dem	Active Gen/Dem

3-3-From Operational Centrality to Holistic Centrality

As previously mentioned, different operational centralities can be derived from a power grid based on the chosen graph (either original or holistic) and the energy flows (either active or reactive) analyzed through various power flow methods (AC or DC). We will categorize these operational centralities accordingly. For flows obtained through AC power flow analysis, we will refer to them simply as active or reactive centrality, such as active betweenness (C_B^P) and reactive betweenness (C_B^Q). In contrast, for flows derived from the DC load flow method, which only provides active flows, we will denote these centralities by the power flow method, such as DC betweenness (C_B^{dc}). When centralities are derived from a holistic graph, we will prefix their notation with "holistic", resulting in terms like active holistic betweenness ($\overset{H}{C}_B^P$), reactive holistic betweenness ($\overset{H}{C}_B^Q$), and DC holistic betweenness ($\overset{H}{C}_B^{dc}$). To streamline our terminology, we will omit the word "operational" from all centrality types, as the flow type (active/reactive) or the power flow method (DC) inherently indicates their operational nature. Table 2 summarizes all centrality measures used in complex power networks.

Various betweenness centralities, as the sum of various dependency matrices, derived from IEEE 14-bus system (Fig. 1) in normal operation condition are calculated and summarized in Table 3. Additionally, the DC holistic betweenness (represented by $\overset{H}{C}_B^{dc}$) has been included in this table for comparison with the

10.22060/EEJ.2025.24278.5667

results presented in [1]. Notably, the new centrality measure closely aligns with the active holistic betweenness, exhibiting a similar trend throughout.

Table 3. Different betweennesses for IEEE 14-bus case

Bus No.	Grap.	Struc.	Operational		Holistic		
	C_B	C_B^S	C_B^P	C_B^Q	$^{H}C_B^P$	$^{H}C_B^Q$	$^{H}C_B^{dc}$
1	0	0	0	0	4	3	4
2	4.7	4.8	5.7	6.1	10.7	10.3	10.7
3	0	0	0	0	3.9	6.8	3.8
4	19.6	21.4	23	22.4	16.9	15.5	17.1
5	16.8	15.2	18.3	17.7	16	14.3	16
6	16	17.2	17.5	14.5	15.9	13.5	15.8
7	9.6	18.6	15	20.8	8	12.5	8
8	0	0	0	0	0	3.3	0
9	16.8	12.4	11.9	7.9	9.8	7.2	9.7
10	3.7	4.8	3	4.8	3.4	4.1	3.4
11	2.9	4.1	3.9	4	3.7	3.1	3.7
12	0	0	0	0	1.8	1.2	1.8
13	4.5	1.4	1.7	1.7	3.5	3.2	3.5
14	5.3	0	0	0	2.4	2	2.4

4. Performance Evaluation through Simulations

This section evaluates the performance of the proposed model through comprehensive simulations, offering insights into its effectiveness across diverse scenarios. It details the experimental setup, provides an in-depth analysis of the simulation results, and compares these outcomes with established benchmarks to highlight the model's strengths and identify critical performance trends.

4-1-Holistic Betweenness Measures vs. Active/Reactive Betweenness Measures

In previous section, we first analyzed the IEEE 14-bus test case under normal operating conditions, calculating both holistic active and reactive, and DC holistic betweenness measures. These results are included in the last two columns of Table 2, alongside previously established operational betweenness measures, with values normalized to sum to 100.

Our findings show that the proposed approach assigns DC holistic betweenness values to buses that previously had zero operational betweenness. Key conclusions include:

1) Holistic measures distribute betweenness impacts more evenly across all system buses compared to traditional operational measures, reflecting that every bus influences active/reactive power flow.
2) A bus that does not contribute to a specific power type (active or reactive) will have a corresponding holistic betweenness of zero. For example, bus 8's active and DC holistic betweenness measures are zero because it is a PV bus with no active power generation or demand.
3) Generation buses typically have higher holistic betweenness values than operational ones due to their crucial role in power flow. For instance, bus 2's active holistic betweenness rises from 5.7% to 10.7%, and its reactive measure increases from 6.1% to 10.3%. Similarly, bus 3's reactive measure goes from 0% to 6.8%.
4) Rankings based on holistic measures may differ from those based on operational betweenness. Bus 4 remains the most critical node in terms of holistic active and reactive betweenness due to its central location, while bus 7's ranking declines as it does not function as a generation or primary load bus.
5) The DC holistic betweenness closely mirrors the active holistic betweenness, exhibiting a similar trend throughout.

Overall, these results underscore the advantages of using holistic measures to better understand the dynamics of power systems and the roles of individual buses within them.

4-2- Correlation of Holistic Betweenness Measures and System States

The previous section has demonstrated the effectiveness of the proposed holistic measures. We have claimed that these measures, when combined with the previously established operational metrics, can effectively capture the dynamics of power grid operations, especially considering that only a limited range of operational conditions was analyzed in previous section and reference [6]. Consequently, the current simulation aims to further validate this claim regarding the proposed holistic measures. To do this,

10.22060/EEJ.2025.24278.5667

we created 10,000 unique operational scenarios by randomly varying generation levels by up to 20% and demand levels by up to 25%, thus generating a wide array of operational cases, which is shown in Fig. 7. The power flow for each scenario was analyzed using both the Newton-Raphson (NR) and DC methods using Matpower package [31]. Using the flow data obtained from these methods, we calculated active and reactive betweenness, as well as active and reactive holistic betweenness, and DC holistic betweenness for each scenario. We then examined the correlations between these various measures and the state information (voltage phase and magnitude), presenting our findings in Tables 4 to 13. Additionally, we implemented a color-coded indicator to visually represent these correlations: negative correlations are indicated in green, positive correlations in red, and weak correlations approach white.

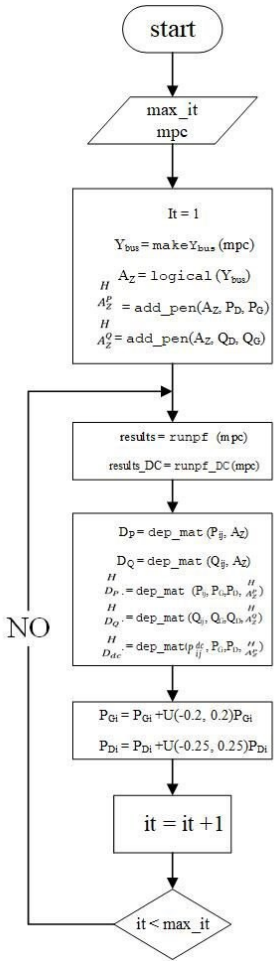

Fig. 7. Flowchart of Generating Different Operational Conditions

10.22060/EEJ.2025.24278.5667

The observations derived from the correlation tables are noteworthy. The bright green and red colors observed in the columns for buses 1, 3, 12, and 14 in Tables 5 and 6 indicate that the newly assigned betweenness values (active holistic and DC holistic betweenness measures) successfully capture the dynamics of system states. Previous findings suggest a strong correlation between active power and voltage phase; this is corroborated by the bright colors in Tables 4 to 6, confirming the relationship between active operational measures and voltage phase, as well as between active/DC holistic measures and voltage phase. Similarly, a strong correlation exists between reactive power and voltage magnitude, which is also validated in Tables 12 and 13.

Notably, some generation buses (such as buses 1 and 3) exhibited traditionally zero measures (refer to Table 4). However, their holistic measures (Tables 5 and 6) are not only non-zero but also display bright colors, underscoring the critical role of generation buses in state dynamics; a role effectively captured by active/DC holistic betweenness. A comparable analysis applies to holistic reactive betweenness and voltage magnitude, as exemplified by bus 9 in Table 13. Our findings reveal a weak correlation between traditional and holistic active measures with voltage magnitudes (light colors in Tables 7 to 9), which aligns with existing knowledge. In contrast, both reactive measures and voltage phase demonstrate an acceptable level of correlation, warranting careful examination in future research.

In summary, our thorough analysis demonstrates that holistic measures (active, reactive, and DC) are more effective than traditional operational metrics in understanding the complex dynamics of power grid operations. These holistic metrics reveal previously overlooked effects of different buses on system behavior, indicating their potential to improve decision-making and grid management strategies. Specifically, operational and holistic centralities can be integrated into AI algorithms to estimate and forecast grid operational parameters, as previously suggested in [10]. The following section will introduce two AI method aimed at accelerating the calculation of active holistic centralities, and estimating voltage magnitudes from DC load flow results. Note that for the next section, no specific feature extraction

10.22060/EEJ.2025.24278.5667

techniques, such as principal component analysis (PCA), were applied; instead, feature selection was guided by the correlation insights from Tables 4 to 13.

Table 4. Correlation between Active Betweenness and Voltage Phase

	$C_B^P(1)$	$C_B^P(2)$	$C_B^P(3)$	$C_B^P(4)$	$C_B^P(5)$	$C_B^P(6)$	$C_B^P(7)$	$C_B^P(8)$	$C_B^P(9)$	$C_B^P(10)$	$C_B^P(11)$	$C_B^P(12)$	$C_B^P(13)$	$C_B^P(14)$
δ_1														
δ_2		-0.57		-0.55	-0.65	0.56	0.54		0.30	0.12	-0.36		-0.66	
δ_3		-0.66		-0.64	-0.73	0.58	0.65		0.44	0.08	-0.34		-0.74	
δ_4		-0.53		-0.54	-0.60	0.57	0.48		0.24	0.14	-0.38		-0.61	
δ_5		-0.49		-0.51	-0.57	0.53	0.45		0.23	0.15	-0.36		-0.58	
δ_6		-0.24		-0.26	-0.33	0.28	0.23		0.07	0.17	-0.24		-0.34	
δ_7		-0.29		-0.32	-0.38	0.44	0.25		0.06	0.22	-0.42		-0.39	
δ_8		-0.29		-0.32	-0.38	0.44	0.25		0.06	0.22	-0.42		-0.39	
δ_9		-0.19		-0.22	-0.28	0.37	0.14		-0.02	0.25	-0.43		-0.29	
δ_{10}		-0.18		-0.21	-0.27	0.36	0.15		0.01	0.21	-0.40		-0.28	
δ_{11}		-0.21		-0.23	-0.30	0.32	0.19		0.04	0.19	-0.34		-0.31	
δ_{12}		-0.21		-0.24	-0.31	0.23	0.20		0.05	0.18	-0.20		-0.31	
δ_{13}		-0.20		-0.23	-0.30	0.23	0.18		0.03	0.19	-0.20		-0.30	
δ_{14}		-0.16		-0.19	-0.26	0.26	0.11		-0.04	0.27	-0.30		-0.26	

Table 5. Correlation between Active Holistic Betweenness and Voltage Phase

	$H_{C_B^P}(1)$	$H_{C_B^P}(2)$	$H_{C_B^P}(3)$	$H_{C_B^P}(4)$	$H_{C_B^P}(5)$	$H_{C_B^P}(6)$	$H_{C_B^P}(7)$	$H_{C_B^P}(8)$	$H_{C_B^P}(9)$	$H_{C_B^P}(10)$	$H_{C_B^P}(11)$	$H_{C_B^P}(12)$	$H_{C_B^P}(13)$	$H_{C_B^P}(14)$
δ_1														
δ_2	-0.63	-0.52	-0.57	-0.23	-0.61	0.50	0.52		0.43	0.10	-0.33	0.02	-0.35	-0.01
δ_3	-0.74	-0.64	-0.71	-0.20	-0.58	0.54	0.59		0.49	0.05	-0.32	-0.02	-0.39	-0.03
δ_4	-0.59	-0.52	-0.52	-0.31	-0.60	0.51	0.51		0.43	0.13	-0.35	0.04	-0.34	0.01
δ_5	-0.56	-0.48	-0.50	-0.28	-0.57	0.48	0.47		0.39	0.13	-0.33	0.04	-0.33	0.01
δ_6	-0.33	-0.22	-0.30	-0.12	-0.37	0.24	0.23		0.16	0.18	-0.21	0.05	-0.27	0.02
δ_7	-0.37	-0.30	-0.34	-0.15	-0.40	0.42	0.27		0.19	0.21	-0.40	0.13	-0.25	0.05
δ_8	-0.37	-0.30	-0.34	-0.15	-0.40	0.42	0.27		0.19	0.21	-0.40	0.13	-0.25	0.05
δ_9	-0.27	-0.20	-0.25	-0.08	-0.31	0.38	0.16		0.09	0.24	-0.41	0.17	-0.21	0.06
δ_{10}	-0.26	-0.19	-0.25	-0.07	-0.30	0.36	0.16		0.11	0.19	-0.38	0.16	-0.20	0.06
δ_{11}	-0.29	-0.20	-0.27	-0.09	-0.33	0.30	0.19		0.13	0.19	-0.31	0.11	-0.23	0.04
δ_{12}	-0.30	-0.19	-0.28	-0.10	-0.34	0.20	0.20		0.14	0.19	-0.17	-0.01	-0.27	0.02
δ_{13}	-0.29	-0.18	-0.27	-0.09	-0.33	0.19	0.19		0.12	0.20	-0.18	0.03	-0.31	0.01
δ_{14}	-0.23	-0.14	-0.22	-0.05	-0.27	0.25	0.12		0.08	0.26	-0.28	0.13	-0.26	-0.11

Table 6. Correlation between DC Holistic Betweenness and Voltage Phase

	$H_{C_B^{dc}}(1)$	$H_{C_B^{dc}}(2)$	$H_{C_B^{dc}}(3)$	$H_{C_B^{dc}}(4)$	$H_{C_B^{dc}}(5)$	$H_{C_B^{dc}}(6)$	$H_{C_B^{dc}}(7)$	$H_{C_B^{dc}}(8)$	$H_{C_B^{dc}}(9)$	$H_{C_B^{dc}}(10)$	$H_{C_B^{dc}}(11)$	$H_{C_B^{dc}}(12)$	$H_{C_B^{dc}}(13)$	$H_{C_B^{dc}}(14)$
δ_1														
δ_2	-0.61	-0.55	-0.56	-0.27	-0.62	0.5	0.53		0.45	0.11	-0.3	-0.02	-0.33	-0.01
δ_3	-0.72	-0.66	-0.7	-0.24	-0.59	0.54	0.59		0.5	0.07	-0.28	-0.05	-0.36	-0.03
δ_4	-0.58	-0.54	-0.52	-0.36	-0.61	0.52	0.51		0.44	0.14	-0.32	0.01	-0.31	0.01
δ_5	-0.55	-0.5	-0.49	-0.32	-0.58	0.48	0.48		0.41	0.15	-0.3	0.01	-0.31	0.01
δ_6	-0.31	-0.24	-0.29	-0.16	-0.38	0.25	0.23		0.17	0.19	-0.18	0.02	-0.25	0.02
δ_7	-0.35	-0.31	-0.33	-0.19	-0.42	0.42	0.27		0.21	0.23	-0.37	0.09	-0.24	0.05
δ_8	-0.35	-0.31	-0.33	-0.19	-0.42	0.42	0.27		0.21	0.23	-0.37	0.09	-0.24	0.05
δ_9	-0.25	-0.21	-0.24	-0.12	-0.32	0.37	0.16		0.1	0.27	-0.39	0.13	-0.2	0.06
δ_{10}	-0.24	-0.2	-0.24	-0.11	-0.31	0.36	0.17		0.12	0.22	-0.36	0.13	-0.2	0.06
δ_{11}	-0.27	-0.22	-0.26	-0.13	-0.34	0.31	0.2		0.14	0.21	-0.28	0.08	-0.22	0.05
δ_{12}	-0.28	-0.21	-0.27	-0.14	-0.35	0.2	0.2		0.14	0.2	-0.14	-0.04	-0.26	0.02
δ_{13}	-0.27	-0.19	-0.26	-0.13	-0.34	0.2	0.19		0.13	0.21	-0.15	0	-0.29	0.01
δ_{14}	-0.21	-0.15	-0.21	-0.1	-0.28	0.26	0.13		0.09	0.28	-0.26	0.09	-0.26	-0.11

10.22060/EEJ.2025.24278.5667

Table 7. Correlation between Active Betweenness and Voltage Magnitude

	$C_B^P(1)$	$C_B^P(2)$	$C_B^P(3)$	$C_B^P(4)$	$C_B^P(5)$	$C_B^P(6)$	$C_B^P(7)$	$C_B^P(8)$	$C_B^P(9)$	$C_B^P(10)$	$C_B^P(11)$	$C_B^P(12)$	$C_B^P(13)$	$C_B^P(14)$
$\|V_1\|$		0.00		0.00	0.00	0.00	0.00		0.00	0.00	0.00		0.00	
$\|V_2\|$		0.00		0.00	0.00	0.00	0.00		0.00	0.00	0.00		0.00	
$\|V_3\|$		0.00		0.00	0.00	0.00	0.00		0.00	0.00	0.00		0.00	
$\|V_4\|$		-0.01		-0.09	-0.07	0.26	-0.04		-0.17	0.24	-0.34		-0.08	
$\|V_5\|$		-0.01		-0.08	-0.07	0.20	-0.03		-0.15	0.23	-0.29		-0.09	
$\|V_6\|$		0.00		0.00	0.00	0.00	0.00		0.00	0.00	0.00		0.00	
$\|V_7\|$		0.11		0.06	0.07	0.08	-0.11		-0.13	0.23	-0.35		0.06	
$\|V_8\|$		0.00		0.00	0.00	0.00	0.00		0.00	0.00	0.00		0.00	
$\|V_9\|$		0.10		0.07	0.07	0.04	-0.08		-0.08	0.19	-0.31		0.07	
$\|V_{10}\|$		0.14		0.11	0.10	0.05	-0.08		-0.05	0.11	-0.32		0.10	
$\|V_{11}\|$		0.15		0.12	0.12	0.06	-0.09		-0.05	0.11	-0.36		0.11	
$\|V_{12}\|$		0.10		0.09	0.07	-0.31	-0.11		-0.10	0.06	0.33		0.09	
$\|V_{13}\|$		0.16		0.14	0.12	-0.33	-0.18		-0.17	0.16	0.25		0.14	
$\|V_{14}\|$		0.14		0.11	0.10	-0.14	-0.18		-0.20	0.29	-0.09		0.11	

Table 8. Correlation between Active Holistic Betweenness and Voltage Magnitude

	$H\ C_B^P(1)$	$H\ C_B^P(2)$	$H\ C_B^P(3)$	$H\ C_B^P(4)$	$H\ C_B^P(5)$	$H\ C_B^P(6)$	$H\ C_B^P(7)$	$H\ C_B^P(8)$	$H\ C_B^P(9)$	$H\ C_B^P(10)$	$H\ C_B^P(11)$	$H\ C_B^P(12)$	$H\ C_B^P(13)$	$H\ C_B^P(14)$
$\|V_1\|$	0.00	0.00	0.00	0.00	0.00	0.00	0.00		0.00	0.00	0.00	0.00	0.00	0.00
$\|V_2\|$	0.00	0.00	0.00	0.00	0.00	0.00	0.00		0.00	0.00	0.00	0.00	0.00	0.00
$\|V_3\|$	0.00	0.00	0.00	0.00	0.00	0.00	0.00		0.00	0.00	0.00	0.00	0.00	0.00
$\|V_4\|$	-0.03	-0.05	0.04	-0.29	-0.25	0.24	0.10		0.09	0.22	-0.35	0.19	-0.10	0.08
$\|V_5\|$	-0.05	-0.04	0.01	-0.21	-0.23	0.18	0.07		0.06	0.23	-0.29	0.16	-0.13	0.07
$\|V_6\|$	0.00	0.00	0.00	0.00	0.00	0.00	0.00		0.00	0.00	0.00	0.00	0.00	0.00
$\|V_7\|$	0.10	0.09	0.10	-0.01	0.00	0.12	-0.05		-0.03	0.19	-0.39	0.23	-0.05	0.07
$\|V_8\|$	0.00	0.00	0.00	0.00	0.00	0.00	0.00		0.00	0.00	0.00	0.00	0.00	0.00
$\|V_9\|$	0.10	0.09	0.09	0.04	0.04	0.08	-0.05		-0.02	0.15	-0.36	0.20	-0.04	0.06
$\|V_{10}\|$	0.13	0.12	0.11	0.08	0.08	0.10	-0.06		-0.02	0.05	-0.36	0.23	-0.01	0.08
$\|V_{11}\|$	0.15	0.14	0.12	0.11	0.10	0.11	-0.06		-0.02	0.05	-0.41	0.25	0.02	0.08
$\|V_{12}\|$	0.11	0.20	0.09	0.10	0.08	-0.32	-0.10		-0.10	0.08	0.28	-0.61	-0.03	-0.01
$\|V_{13}\|$	0.16	0.25	0.13	0.13	0.11	-0.33	-0.17		-0.16	0.17	0.20	-0.09	-0.43	-0.12
$\|V_{14}\|$	0.18	0.21	0.15	0.13	0.12	-0.10	-0.15		-0.10	0.27	-0.14	0.16	-0.18	-0.40

Table 9. Correlation between DC Holistic Betweenness and Voltage Magnitude

	$H\ C_B^{dc}(1)$	$H\ C_B^{dc}(2)$	$H\ C_B^{dc}(3)$	$H\ C_B^{dc}(4)$	$H\ C_B^{dc}(5)$	$H\ C_B^{dc}(6)$	$H\ C_B^{dc}(7)$	$H\ C_B^{dc}(8)$	$H\ C_B^{dc}(9)$	$H\ C_B^{dc}(10)$	$H\ C_B^{dc}(11)$	$H\ C_B^{dc}(12)$	$H\ C_B^{dc}(13)$	$H\ C_B^{dc}(14)$
$\|V_1\|$	0	0	0	0	0	0	0		0	0	0	0	0	0
$\|V_2\|$	0	0	0	0	0	0	0		0	0	0	0	0	0
$\|V_3\|$	0	0	0	0	0	0	0		0	0	0	0	0	0
$\|V_4\|$	-0.03	-0.06	0.05	-0.33	-0.28	0.27	0.08		0.08	0.25	-0.31	0.16	-0.08	0.08
$\|V_5\|$	-0.04	-0.05	0.01	-0.26	-0.26	0.21	0.06		0.05	0.24	-0.25	0.13	-0.11	0.07
$\|V_6\|$	0	0	0	0	0	0	0		0	0	0	0	0	0
$\|V_7\|$	0.09	0.06	0.1	-0.07	-0.05	0.2	-0.08		-0.08	0.2	-0.32	0.19	-0.01	0.07
$\|V_8\|$	0	0	0	0	0	0	0		0	0	0	0	0	0
$\|V_9\|$	0.09	0.05	0.08	-0.01	0	0.18	-0.08		-0.08	0.16	-0.29	0.17	0	0.06
$\|V_{10}\|$	0.12	0.09	0.1	0.03	0.04	0.19	-0.09		-0.07	0.06	-0.29	0.2	0.03	0.08
$\|V_{11}\|$	0.14	0.1	0.11	0.06	0.06	0.2	-0.1		-0.07	0.06	-0.34	0.22	0.06	0.08
$\|V_{12}\|$	0.11	0.17	0.09	0.08	0.07	-0.29	-0.11		-0.11	0.06	0.3	-0.61	-0.04	-0.01
$\|V_{13}\|$	0.16	0.22	0.13	0.1	0.1	-0.29	-0.18		-0.18	0.16	0.23	-0.1	-0.43	-0.12
$\|V_{14}\|$	0.17	0.18	0.14	0.08	0.09	-0.03	-0.17		-0.12	0.26	-0.09	0.14	-0.16	-0.4

Table 10. Correlation between Reactive Betweenness and Voltage Phase

	$C_B^Q(1)$	$C_B^Q(2)$	$C_B^Q(3)$	$C_B^Q(4)$	$C_B^Q(5)$	$C_B^Q(6)$	$C_B^Q(7)$	$C_B^Q(8)$	$C_B^Q(9)$	$C_B^Q(10)$	$C_B^Q(11)$	$C_B^Q(12)$	$C_B^Q(13)$	$C_B^Q(14)$
δ_1														
δ_2		-0.73		-0.50	-0.46	0.72	0.57		0.05	-0.15	-0.14		-0.86	
δ_3		-0.70		-0.54	-0.44	0.64	0.70		0.05	-0.16	-0.10		-0.80	
δ_4		-0.74		-0.52	-0.43	0.81	0.44		0.06	-0.14	-0.15		-0.89	
δ_5		-0.74		-0.51	-0.45	0.83	0.42		0.06	-0.13	-0.17		-0.89	
δ_6		-0.72		-0.41	-0.48	0.92	0.21		0.05	-0.08	-0.25		-0.87	
δ_7		-0.73		-0.43	-0.46	0.89	0.25		0.04	-0.14	-0.14		-0.89	
δ_8		-0.73		-0.43	-0.46	0.89	0.25		0.04	-0.14	-0.14		-0.89	
δ_9		-0.71		-0.37	-0.45	0.90	0.17		0.02	-0.14	-0.13		-0.88	
δ_{10}		-0.71		-0.38	-0.46	0.91	0.17		0.03	-0.12	-0.15		-0.88	
δ_{11}		-0.72		-0.40	-0.48	0.92	0.19		0.04	-0.10	-0.19		-0.88	
δ_{12}		-0.71		-0.41	-0.49	0.92	0.19		0.06	-0.07	-0.26		-0.85	
δ_{13}		-0.70		-0.40	-0.49	0.92	0.17		0.06	-0.08	-0.25		-0.84	
δ_{14}		-0.70		-0.37	-0.47	0.91	0.13		0.04	-0.10	-0.19		-0.84	

Table 11. Correlation between Reactive Holistic Betweenness and Voltage Phase

	$H C_B^Q(1)$	$H C_B^Q(2)$	$H C_B^Q(3)$	$H C_B^Q(4)$	$H C_B^Q(5)$	$H C_B^Q(6)$	$H C_B^Q(7)$	$H C_B^Q(8)$	$H C_B^Q(9)$	$H C_B^Q(10)$	$H C_B^Q(11)$	$H C_B^Q(12)$	$H C_B^Q(13)$	$H C_B^Q(14)$
δ_1														
δ_2	-0.58	-0.66	-0.38	-0.38	0.18	0.75	0.56	0.12	0.12	-0.05	-0.07	-0.04	-0.06	0.03
δ_3	-0.59	-0.63	-0.43	-0.39	0.12	0.69	0.68	0.22	0.12	-0.07	-0.04	-0.04	-0.03	0.03
δ_4	-0.57	-0.66	-0.38	-0.40	0.26	0.81	0.44	0.03	0.13	-0.04	-0.09	-0.03	-0.07	0.04
δ_5	-0.57	-0.66	-0.38	-0.39	0.25	0.82	0.43	0.01	0.12	-0.03	-0.10	-0.03	-0.08	0.04
δ_6	-0.52	-0.62	-0.33	-0.30	0.25	0.86	0.26	-0.13	0.10	0.01	-0.18	0.01	-0.12	0.04
δ_7	-0.54	-0.65	-0.35	-0.32	0.26	0.86	0.28	-0.12	0.08	-0.04	-0.07	-0.03	-0.08	0.04
δ_8	-0.54	-0.65	-0.35	-0.32	0.26	0.86	0.28	-0.12	0.08	-0.04	-0.07	-0.03	-0.08	0.04
δ_9	-0.52	-0.63	-0.33	-0.28	0.26	0.85	0.21	-0.19	0.06	-0.04	-0.07	-0.03	-0.08	0.04
δ_{10}	-0.52	-0.63	-0.33	-0.28	0.26	0.85	0.21	-0.18	0.07	-0.03	-0.08	-0.03	-0.09	0.04
δ_{11}	-0.52	-0.63	-0.33	-0.30	0.25	0.86	0.23	-0.16	0.09	-0.01	-0.12	-0.01	-0.10	0.04
δ_{12}	-0.50	-0.61	-0.33	-0.30	0.24	0.85	0.24	-0.14	0.11	0.01	-0.19	0.01	-0.11	0.04
δ_{13}	-0.50	-0.61	-0.32	-0.30	0.23	0.86	0.22	-0.15	0.11	0.00	-0.18	0.03	-0.10	0.04
δ_{14}	-0.50	-0.61	-0.32	-0.27	0.24	0.85	0.18	-0.19	0.08	-0.02	-0.12	0.01	-0.09	0.07

Table 12. Correlation between Reactive Betweenness and Voltage Magnitude

	$C_B^Q(1)$	$C_B^Q(2)$	$C_B^Q(3)$	$C_B^Q(4)$	$C_B^Q(5)$	$C_B^Q(6)$	$C_B^Q(7)$	$C_B^Q(8)$	$C_B^Q(9)$	$C_B^Q(10)$	$C_B^Q(11)$	$C_B^Q(12)$	$C_B^Q(13)$	$C_B^Q(14)$
$\|V_1\|$		0.00		0.00	0.00	0.00	0.00		0.00	0.00	0.00		0.00	
$\|V_2\|$		0.00		0.00	0.00	0.00	0.00		0.00	0.00	0.00		0.00	
$\|V_3\|$		0.00		0.00	0.00	0.00	0.00		0.00	0.00	0.00		0.00	
$\|V_4\|$		-0.45		-0.02	-0.09	0.75	-0.21		-0.16	0.13	-0.38		-0.63	
$\|V_5\|$		-0.51		-0.10	-0.21	0.84	-0.16		-0.11	0.09	-0.37		-0.69	
$\|V_6\|$		0.00		0.00	0.00	0.00	0.00		0.00	0.00	0.00		0.00	
$\|V_7\|$		-0.22		0.51	0.27	0.39	-0.10		-0.61	0.47	-0.66		-0.33	
$\|V_8\|$		0.00		0.00	0.00	0.00	0.00		0.00	0.00	0.00		0.00	
$\|V_9\|$		-0.13		0.62	0.37	0.22	-0.03		-0.69	0.54	-0.70		-0.19	
$\|V_{10}\|$		-0.11		0.63	0.39	0.26	-0.01		-0.70	0.41	-0.65		-0.16	
$\|V_{11}\|$		-0.12		0.61	0.37	0.27	-0.01		-0.68	0.38	-0.64		-0.17	
$\|V_{12}\|$		-0.11		0.09	-0.06	0.20	-0.11		-0.12	0.28	-0.30		-0.16	
$\|V_{13}\|$		-0.17		0.17	-0.06	0.29	-0.15		-0.22	0.38	-0.37		-0.21	
$\|V_{14}\|$		-0.16		0.42	0.16	0.28	-0.11		-0.49	0.48	-0.54		-0.22	

Table 13. Correlation between Reactive Holistic Betweenness and Voltage Magnitude

	$H C_B^Q(1)$	$H C_B^Q(2)$	$H C_B^Q(3)$	$H C_B^Q(4)$	$H C_B^Q(5)$	$H C_B^Q(6)$	$H C_B^Q(7)$	$H C_B^Q(8)$	$H C_B^Q(9)$	$H C_B^Q(10)$	$H C_B^Q(11)$	$H C_B^Q(12)$	$H C_B^Q(13)$	$H C_B^Q(14)$
$\|V_1\|$	0.00	0.00	0.00	0.00	0.00	0.00	0.00	0.00	0.00	0.00	0.00	0.00	0.00	0.00
$\|V_2\|$	0.00	0.00	0.00	0.00	0.00	0.00	0.00	0.00	0.00	0.00	0.00	0.00	0.00	0.00
$\|V_3\|$	0.00	0.00	0.00	0.00	0.00	0.00	0.00	0.00	0.00	0.00	0.00	0.00	0.00	0.00
$\|V_4\|$	-0.27	-0.41	-0.14	0.01	0.55	0.62	-0.11	-0.50	-0.18	0.13	-0.34	0.08	-0.25	0.03
$\|V_5\|$	-0.31	-0.46	-0.18	-0.06	0.47	0.70	-0.07	-0.45	-0.11	0.11	-0.32	0.07	-0.23	0.03
$\|V_6\|$	0.00	0.00	0.00	0.00	0.00	0.00	0.00	0.00	0.00	0.00	0.00	0.00	0.00	0.00
$\|V_7\|$	-0.16	-0.23	-0.09	0.54	0.70	0.24	0.11	-0.70	-0.69	0.33	-0.69	0.25	-0.46	-0.03
$\|V_8\|$	0.00	0.00	0.00	0.00	0.00	0.00	0.00	0.00	0.00	0.00	0.00	0.00	0.00	0.00
$\|V_9\|$	-0.11	-0.15	-0.07	0.65	0.69	0.09	0.19	-0.68	-0.79	0.36	-0.75	0.28	-0.48	-0.04
$\|V_{10}\|$	-0.09	-0.13	-0.06	0.65	0.70	0.12	0.19	-0.63	-0.79	0.19	-0.72	0.34	-0.44	0.00
$\|V_{11}\|$	-0.09	-0.13	-0.06	0.63	0.69	0.13	0.18	-0.61	-0.76	0.18	-0.72	0.34	-0.42	0.01
$\|V_{12}\|$	-0.02	-0.04	-0.02	0.16	0.24	0.08	0.02	-0.16	-0.10	0.23	-0.29	-0.37	-0.44	-0.08
$\|V_{13}\|$	-0.05	-0.10	-0.04	0.24	0.34	0.12	0.01	-0.30	-0.21	0.30	-0.37	-0.04	-0.66	-0.10
$\|V_{14}\|$	-0.09	-0.14	-0.05	0.47	0.55	0.14	0.09	-0.51	-0.52	0.35	-0.55	0.19	-0.54	-0.34

5. AI-Enhanced Estimation Techniques for Holistic Power Network Analysis

High-level description: This section explores a range of estimation techniques to derive critical power system parameters from DC holistic dependency matrices and betweenness measures, progressing from simple linear regression to sophisticated deep neural networks (DNNs) and convolutional neural networks (CNNs). Subsections 5-2 to 5-4 demonstrate how the proposed holistic dependency matrix and holistic betweenness centrality, calculated as the sum of its columns, effectively extract diverse features such as

active holistic betweenness and voltage magnitudes. Starting with linear regression for baseline predictions, the analysis advances to DNNs for capturing non-linear relationships, and culminates in CNNs to process 2-D dependency matrices as images. These methods are validated across the IEEE 14-bus system, with Subsection 5-5 further proving the scalability of the proposed approaches to the larger IEEE 57-bus system, highlighting their adaptability and robustness for enhanced power network analysis.

5-1- Data Preparation for AI Models

This subsection outlines the data preparation process for training, validating, and testing the AI models used in this study. For the IEEE 14-bus system, we generated 10,000 training samples by randomly varying generation levels by up to 20% and demand levels by up to 25%, as described in Fig. 7. For each scenario, both AC and DC load flow analyses were performed using the Newton-Raphson method and DC approximations, respectively. Algorithm 1 was then applied to derive DC holistic and active holistic betweenness measures from the DC and AC results, respectively, while bus states (voltage magnitudes and phases) were obtained from the AC load flow solutions. This process was repeated to create 1,000 validation samples and 50 test samples, ensuring a comprehensive dataset for model evaluation.

For the IEEE 57-bus system, a similar approach was adopted, generating 8,000 training samples, 800 validation samples, and 100 test samples with the same variation ranges for generation and demand. The same load flow analyses and Algorithm 1 were used to compute the corresponding DC holistic, active holistic betweenness measures, and bus states. No specific feature extraction techniques, such as principal component analysis (PCA), were applied; instead, the selection of input features, particularly DC holistic betweenness, was guided by the correlation insights reported in Tables 4 to 13, which highlight their strong relationships with system states.

5-2- Baseline and DNN-Based Estimation of Active Holistic Betweenness

This subsection explores the use of linear regression to estimate active holistic betweenness measures from DC holistic measures derived from DC power flow results, followed by an evaluation of a deep

neural network (DNN) to enhance prediction accuracy. The input features comprise DC holistic betweenness measures for all 14 buses except bus 8, resulting in 13 inputs, while the outputs are the corresponding active holistic betweenness measures, also totaling 13 features.

5-2-1- Linear Regression Analysis

Linear regression serves as the primary approach, assuming a linear relationship between DC holistic inputs and active holistic outputs. The correlation between these measures is strong, as evidenced by Table 14, where red colors along the main diagonal indicate more than 99% correlation between a bus's active and DC holistic measures. This suggests DC holistics are a reliable proxy for active measures. The regression model was fitted to the training data, achieving mean training RMSE of 0.0223 and R^2 of 0.9928, reflecting high accuracy. Test performance, detailed in Table 15, shows per-bus RMSE ranging from 0.0033 to 0.0584, and R^2 from 0.9906 to 0.9996, with a mean test RMSE of 0.0199, and R^2 of 0.9930. Buses 12 and 11 stand out with the and lowest R^2 (0.9841 and 0.9881), reflecting their distinct topological role and weaker correlation.

5-2-2 Deep Neural Network Enhancement

To capture potential non-linearities, a DNN was developed with an input layer of 13 features, followed by a fully connected layer with 128 neurons and ReLU activation, a second layer with 64 neurons and ReLU activation, a third layer with 64 neurons and ReLU activation, and a fourth layer with 64 neurons and ReLU activation. The output layer, with 13 neurons, uses a regression layer as the loss function. The network was trained on the 10,000 samples using the Adam optimizer, with an initial learning rate of 0.001 reduced by half every 25 epochs, a mini-batch size of 32, L2 regularization of 0.00001, validation patience of 300, and gradient clipping at a threshold of 1. Training ran for a maximum of 150 epochs, stopping at 32,800 iterations (106 epochs) when the validation loss did not improve for 300 iterations, with a final validation loss of 0.0057–0.0064, training RMSE of 0.12, and validation RMSE of 0.11. The training progress is visualized in Fig. 9-(a), showing an initial RMSE drop and stable convergence. Test

10.22060/EEJ.2025.24278.5667

results in Table 15 align with training, with a mean RMSE of 0.0257 and R^2 of 0.98, slightly improving upon linear regression for buses with non-linear patterns. The DNN's mean training RMSE of 0.12, derived from the training curve, compares favorably to the linear regression's mean training RMSE of 0.0223, though the aggregated nature of the DNN metric suggests room for per-bus refinement. This approach enhances prediction accuracy, particularly for buses like 11, where linear regression underperforms.

Table 14. Correlation between Active Holistic Betweenness and DC Holistic Betweenness

	$C_B^{H,P}(1)$	$C_B^{H,P}(2)$	$C_B^{H,P}(3)$	$C_B^{H,P}(4)$	$C_B^{H,P}(5)$	$C_B^{H,P}(6)$	$C_B^{H,P}(7)$	$C_B^{H,P}(8)$	$C_B^{H,P}(9)$	$C_B^{H,P}(10)$	$C_B^{H,P}(11)$	$C_B^{H,P}(12)$	$C_B^{H,P}(13)$	$C_B^{H,P}(14)$
$C_B^{H,dc}(1)$	0.998	0.956	0.876	0.608	0.858	-0.52	-0.888	0	-0.766	-0.021	0.034	0.243	0.392	0.071
$C_B^{H,dc}(2)$	0.956	0.997	0.824	0.681	0.844	-0.66	-0.916	0	-0.82	-0.003	0.187	0.171	0.348	0.047
$C_B^{H,dc}(3)$	0.871	0.823	0.999	0.351	0.673	-0.472	-0.749	0	-0.64	0.012	0.059	0.2	0.347	0.07
$C_B^{H,dc}(4)$	0.615	0.67	0.357	0.996	0.809	-0.371	-0.731	0	-0.691	-0.107	0.008	0.154	0.211	0.013
$C_B^{H,dc}(5)$	0.865	0.855	0.68	0.809	0.997	-0.488	-0.873	0	-0.782	-0.103	0.054	0.205	0.34	0.03
$C_B^{H,dc}(6)$	-0.526	-0.642	-0.477	-0.361	-0.487	0.992	0.578	0	0.561	-0.051	-0.772	0.202	-0.097	0.085
$C_B^{H,dc}(7)$	-0.891	-0.917	-0.751	-0.737	-0.869	0.593	0.999	0	0.961	-0.247	-0.052	-0.218	-0.332	-0.086
$C_B^{H,dc}(8)$	0	0	0	0	0	0	0	0	0	0	0	0	0	0
$C_B^{H,dc}(9)$	-0.768	-0.818	-0.642	-0.698	-0.777	0.584	0.964	0	0.997	-0.384	-0.046	-0.16	-0.273	-0.176
$C_B^{H,dc}(10)$	-0.036	-0.009	0	-0.119	-0.12	-0.122	-0.238	0	-0.359	0.986	-0.182	-0.104	-0.209	-0.175
$C_B^{H,dc}(11)$	0.075	0.209	0.094	0.041	0.099	-0.791	-0.095	0	-0.09	-0.233	0.993	-0.405	-0.093	-0.179
$C_B^{H,dc}(12)$	0.222	0.153	0.18	0.14	0.179	0.261	-0.2	0	-0.149	-0.016	-0.484	0.991	0.161	-0.017
$C_B^{H,dc}(13)$	0.403	0.358	0.357	0.223	0.352	-0.07	-0.346	0	-0.296	-0.173	-0.151	0.199	0.992	0.213
$C_B^{H,dc}(14)$	0.078	0.057	0.075	0.017	0.036	0.082	-0.091	0	-0.197	-0.151	-0.186	-0.021	0.207	1

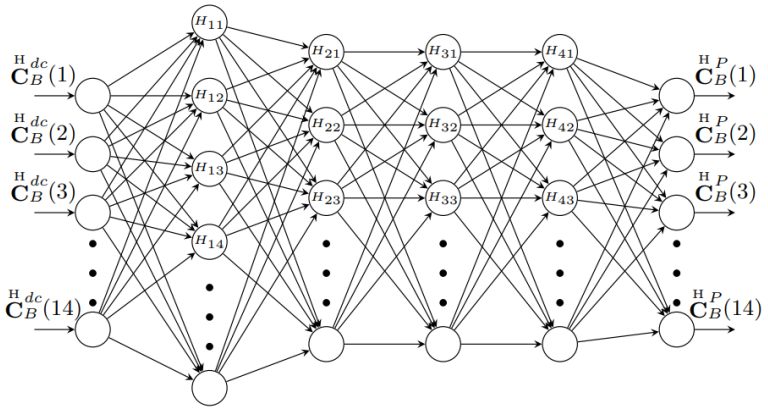

Fig. 8. Structure of the deep neural network used for active holistic prediction.

10.22060/EEJ.2025.24278.5667

Table 15. Performance metrics of linear regression (training and test) and DNN (test) for active holistic prediction across 14 buses.

Bus	Linear Regression (Training)		Linear Regression (Test)		DNN (Test)	
	RMSE	R^2	RMSE	R^2	RMSE	R^2
$C_B^{H,P}(1)$	0.0035	0.9977	0.0033	0.9971	0.0142	0.9463
$C_B^{H,P}(2)$	0.0178	0.9956	0.0198	0.9913	0.0287	0.9818
$C_B^{H,P}(3)$	0.0037	0.9988	0.0043	0.9974	0.0209	0.9379
$C_B^{H,P}(4)$	0.0205	0.9935	0.0169	0.9926	0.0197	0.9899
$C_B^{H,P}(5)$	0.0165	0.9956	0.0160	0.9932	0.0166	0.9927
$C_B^{H,P}(6)$	0.0455	0.9862	0.0339	0.9906	0.0374	0.9886
$C_B^{H,P}(7)$	0.0221	0.9982	0.0177	0.9983	0.0219	0.9974
$C_B^{H,P}(9)$	0.0216	0.9942	0.0179	0.9941	0.0258	0.9876
$C_B^{H,P}(10)$	0.0633	0.9816	0.0584	0.9902	0.0643	0.9881
$C_B^{H,P}(11)$	0.0505	0.9879	0.0433	0.9881	0.0398	0.9900
$C_B^{H,P}(12)$	0.0135	0.9890	0.0140	0.9841	0.0165	0.9778
$C_B^{H,P}(13)$	0.0081	0.9880	0.0078	0.9923	0.0198	0.9498
$C_B^{H,P}(14)$	0.0035	0.9996	0.0049	0.9996	0.0085	0.9988
Mean	0.0223	0.9928	0.0199	0.9930	0.0257	0.9790

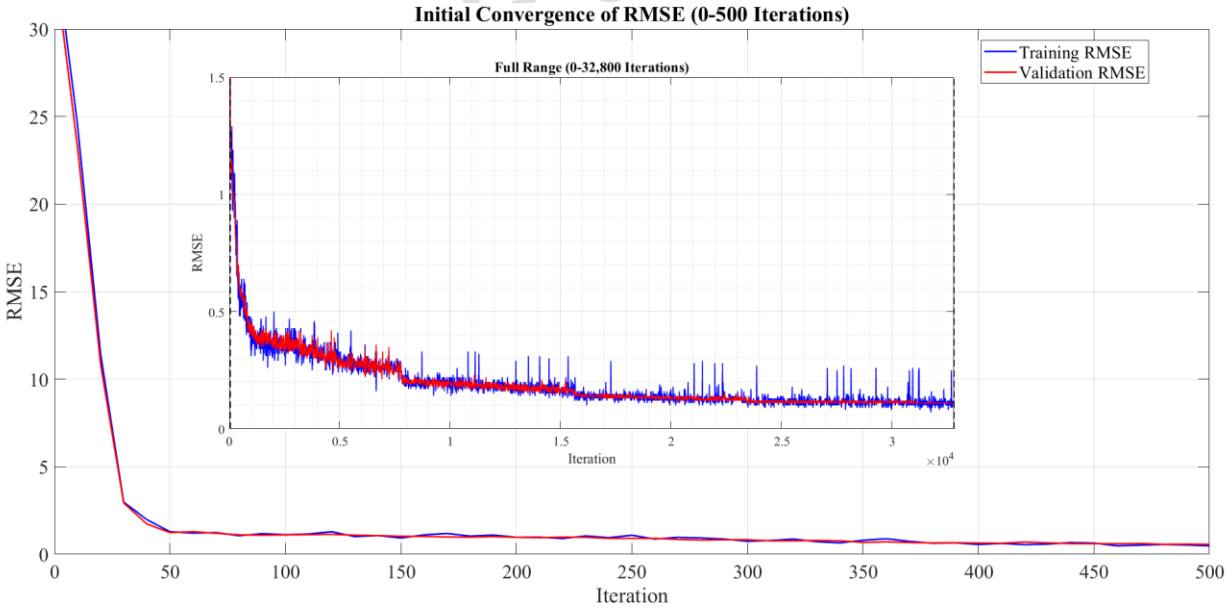

(a)

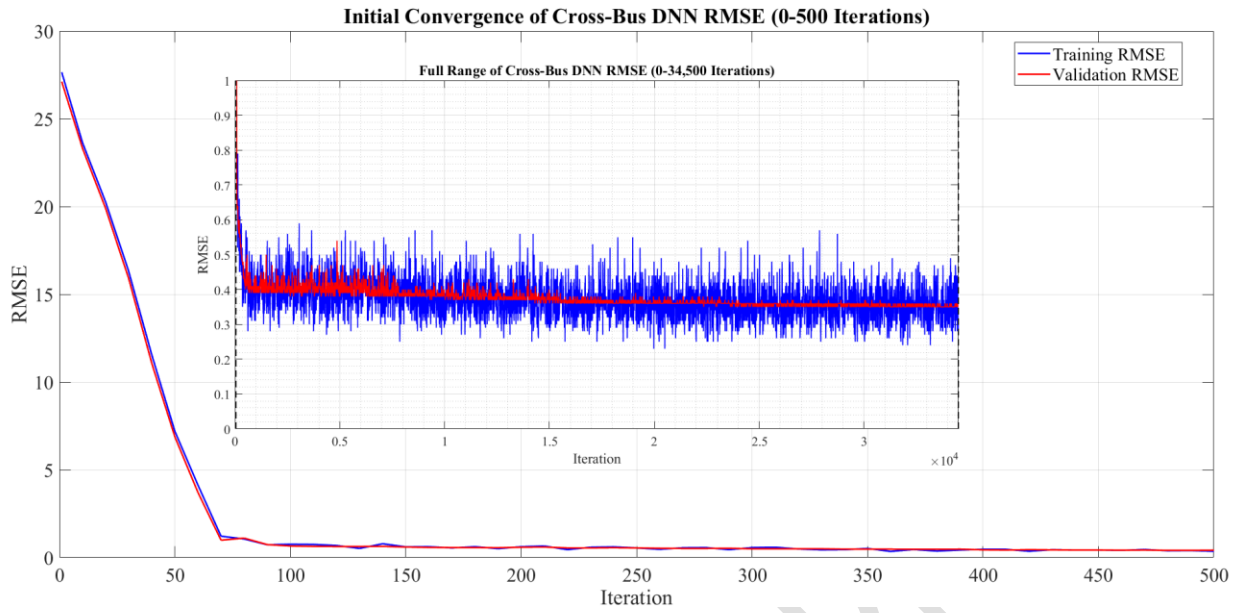

(b)

Fig. 9. Training curve for (a) DNN in Section 5-2-2, showing RMSE convergence over 32,800 iterations; (b) DNN in Section 5-3, illustrating RMSE convergence over 34,800 iterations.

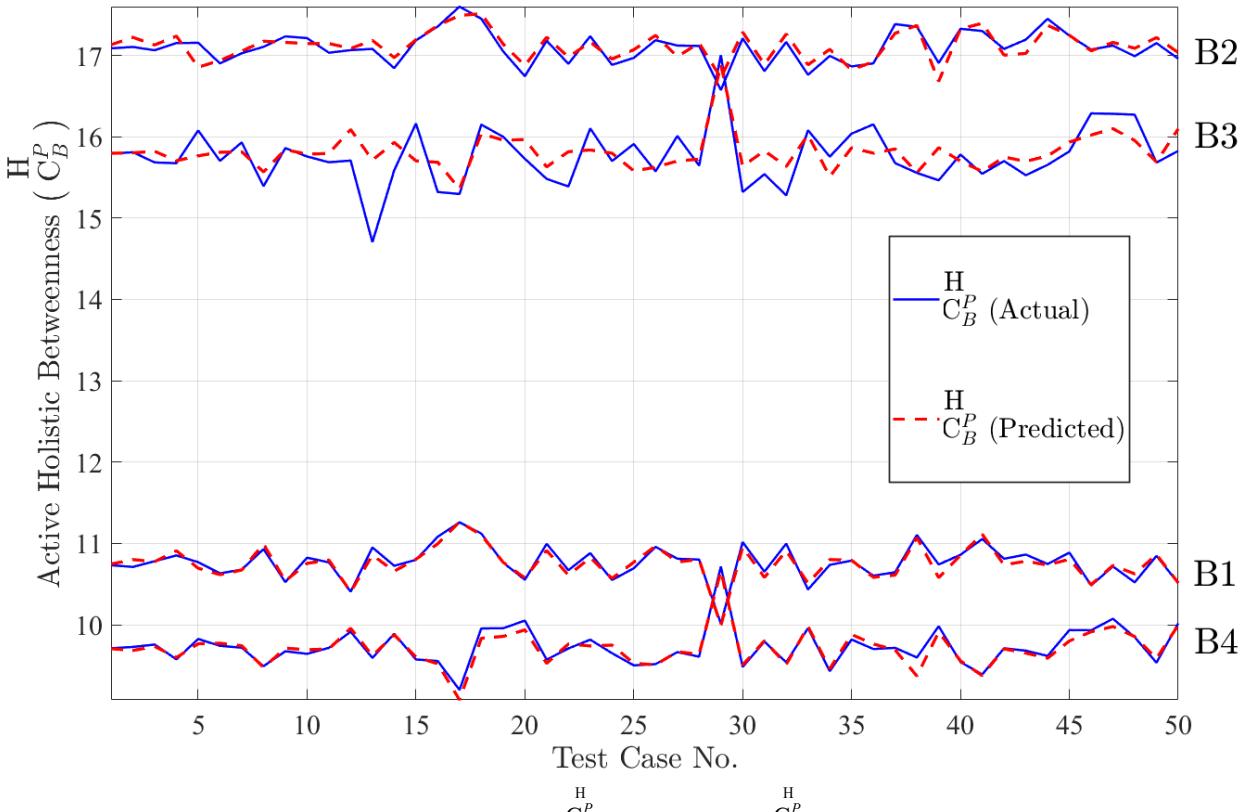

Fig. 10. Cross-bus prediction comparison of actual (C_B^P) and predicted (C_B^P) active holistics for buses 2, 4, 6, and 9.

10.22060/EEJ.2025.24278.5667

5-3- Cross-Bus Prediction of Active Holistics Using DNN

This subsection focuses on predicting active holistic betweenness measures for buses 2, 4, 6, and 9 using input features from the DC holistic betweenness measures of buses 1, 3, 5, and 7, addressing cross-bus dependencies within the 14-bus system. The motivation arises from observing Table 14, where bright red/green block from a_{11} to a_{99} indicates strong correlations between active and DC holistics among buses 1 to 9, primarily along the main diagonal due to intra-bus relationships (the block boarders are bolded in Table 14). However, this strong correlation is not applicable here, as the analysis targets cross-bus prediction, where DC holistics of buses 2, 4, 6, and 9 are excluded as inputs. Instead, the goal is to derive the active holistics of buses 2, 4, 6, and 9 solely from the DC holistics of buses 1, 3, 5, and 7, leveraging potential indirect dependencies. Since bus 8's holistic measure is zero, it is omitted, leaving 13 features, but the prediction focuses on the four specified target buses.

The deep neural network (DNN) architecture builds on the approach from Section 4-1, with layers comprising a feature input layer for 4 inputs, a fully connected layer with 128 neurons and ReLU activation, followed by three fully connected layers with 64 neurons each and ReLU activation, and an output layer with 4 neurons using a regression loss function. Training utilized the Adam optimizer with an initial learning rate of 0.001, reduced by half every 25 epochs via a piecewise schedule, a mini-batch size of 32, L2 regularization of 0.00001 to prevent overfitting, gradient clipping at a threshold of 1, and validation patience of 300. The model was trained for up to 150 epochs, stopping at 34,800 iterations (112 epochs) when the validation loss did not improve for 300 iterations, achieving a validation RMSE of 0.35 and a training RMSE of 0.0599, as shown in the training curve (Fig. 9-(b)). The progress indicates stable convergence with minimal overfitting, supported by a validation RMSE of 0.0599 at the final iteration.

10.22060/EEJ.2025.24278.5667

Table 16. Test performance metrics of DNN and linear regression for cross-bus prediction of active holistics for buses 2, 4, 6, and 9 in IEEE 14-bus System.

Bus	DNN (Test)		Linear Regression (Test)	
	RMSE	R^2	RMSE	R^2
$C_B^{H,P}(2)$	0.0597	0.9214	0.0654	0.9058
$C_B^{H,P}(4)$	0.0842	0.8157	0.1034	0.7225
$C_B^{H,P}(6)$	0.2601	0.4479	0.2727	0.3931
$C_B^{H,P}(9)$	0.0683	0.9134	0.0505	0.9527
Mean	0.1181	0.7746	0.1230	0.7435

Performance metrics, detailed in Table 16, compare the DNN's test results with linear regression. The DNN achieves a mean test RMSE of 0.1181 and R^2 of 0.7746 across buses 2, 4, 6, and 9, with individual RMSE values ranging from 0.0597 (bus 2) to 0.2601 (bus 6) and R^2 from 0.4479 (bus 6) to 0.9214 (bus 2). In contrast, linear regression yields a mean test RMSE of 0.1230 and R^2 of 0.7435, with RMSE from 0.0505 (bus 9) to 0.2727 (bus 6) and R^2 from 0.3931 (bus 6) to 0.9527 (bus 9). The DNN outperforms linear regression, particularly for bus 6, where R^2 improves from 0.3931 to 0.4479 and RMSE decreases from 0.2727 to 0.2601, reflecting the DNN's ability to model non-linear cross-bus dependencies. This advantage is less pronounced for bus 9, where linear regression's R^2 (0.9527) exceeds the DNN's (0.9134), likely due to stronger linear trends in that case.

The mean training RMSE of 0.0599 for the DNN, derived from the training curve, is higher than the linear regression's mean training RMSE of 0.0223 from Section 5-2, reflecting the increased complexity of cross-bus prediction. However, the DNN's test performance validates its effectiveness, setting the stage for further scalability analysis done in 5-5. This performance is visually represented in Fig. 10, which compares the actual active holistic betweenness measures $C_B^{H,P}$ for buses 2, 4, 6, and 9, plotted as solid blue lines, with their predicted counterparts, shown as dashed red lines. The figure highlights the model's ability to approximate the target values across the 50 test samples, with notable alignment for buses 2 and 4, though bus 6 shows greater deviation, consistent with its lower R^2 of 0.4479.

10.22060/EEJ.2025.24278.5667

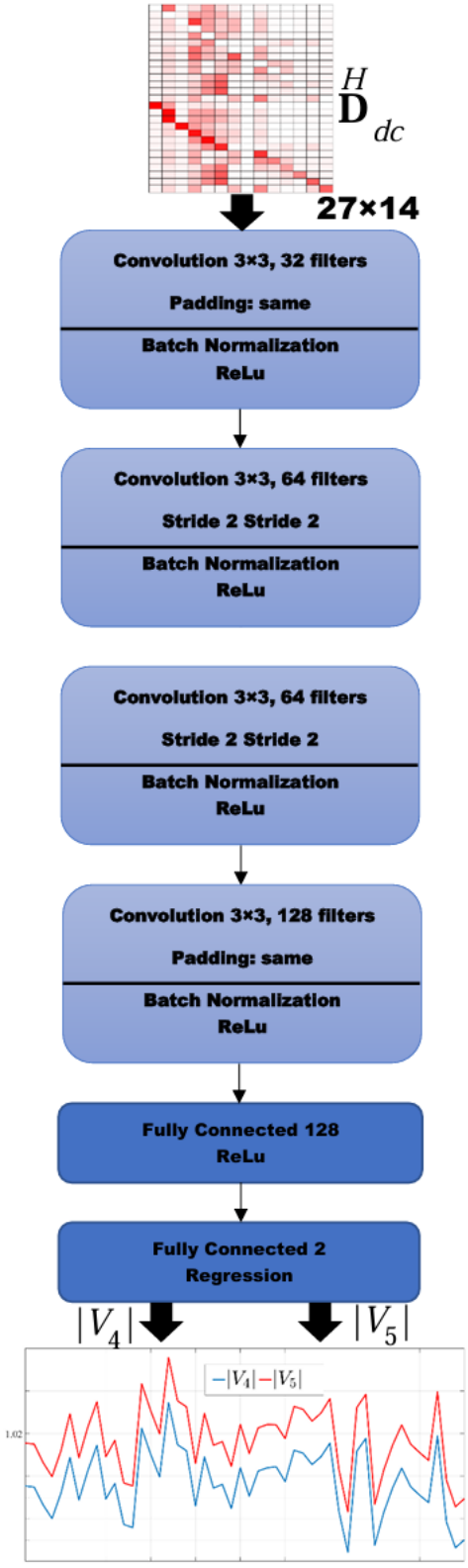

Fig. 11. CNN Architecture for Voltage Magnitude Estimation from DC Holistic Dependency Matrices.

10.22060/EEJ.2025.24278.5667

To optimize the DNN for cross-bus prediction, various activation functions were tested, including sigmoid, Swish, and Leaky ReLU, in addition to the selected ReLU. Our analysis revealed that ReLU consistently delivered the best performance, with a mean test R^2 of 0.7746 and RMSE of 0.1181, outperforming sigmoid (R^2 0.1453, RMSE 0.2236), Swish (R^2 0.7410, RMSE 0.1256), and Leaky ReLU (R^2 0.6995, RMSE 0.1377), due to its ability to handle the non-linear dependencies across buses. This exploration ensured the model's robustness for the task at hand.

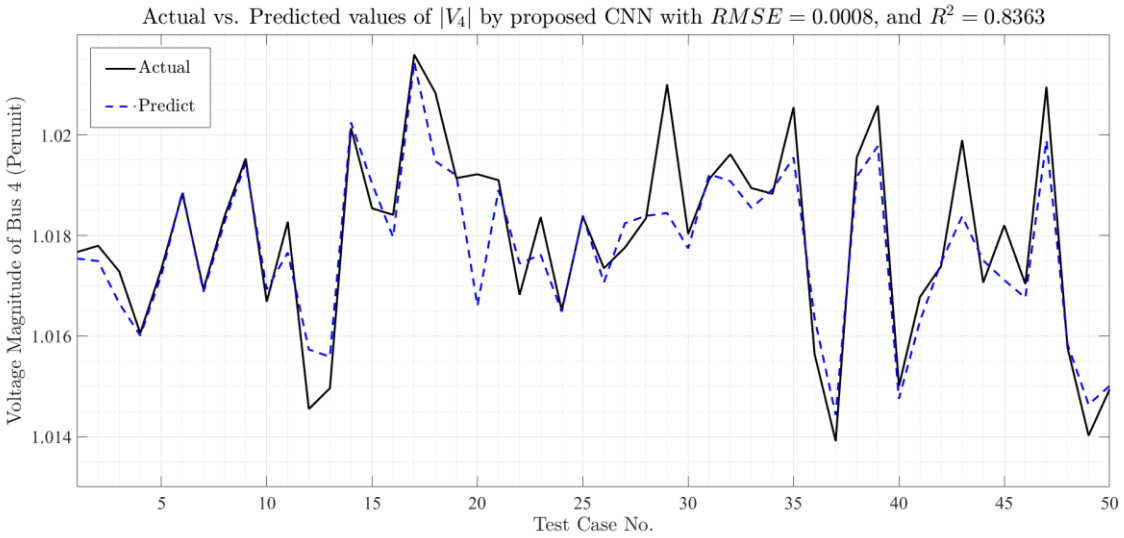

(a)

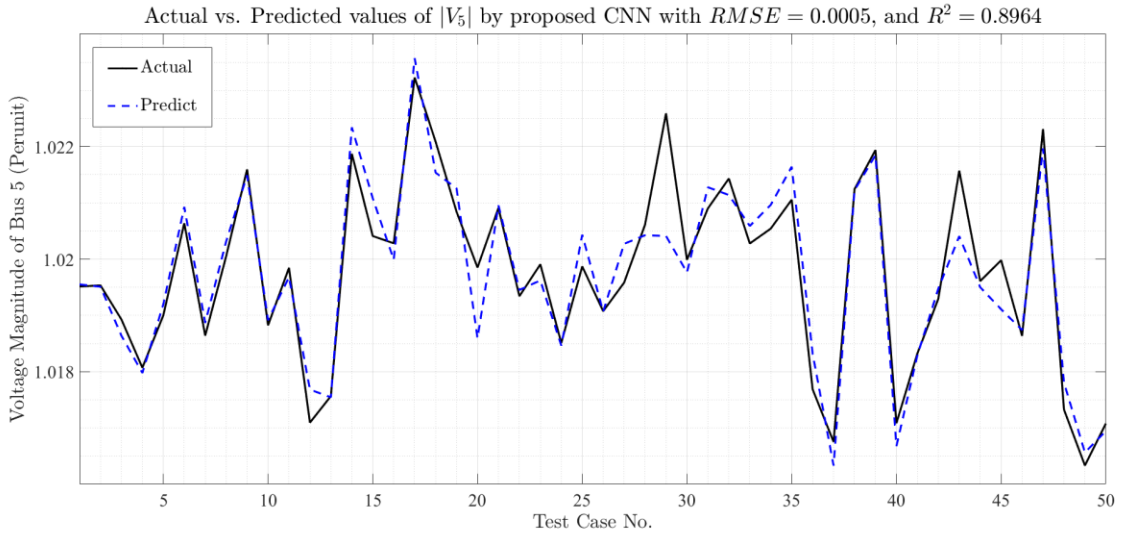

(b)

Fig. 12. Actual vs. estimated voltage magnitudes of buses 4 and 5 using the proposed CNN.

10.22060/EEJ.2025.24278.5667

5-4- CNN-Based Voltage Magnitude Estimation from DC Dependency Matrices

This subsection investigates the estimation of voltage magnitudes for buses 4 and 5 directly from the DC holistic dependency matrix using a convolutional neural network, leveraging the matrix as a 2-D input to capture non-linear grid characteristics from linear DC load flow analysis. Due to the non-sequential nature of our data, a convolutional neural network (CNN) was selected over recurrent neural networks (RNNs) or hybrid CNN-RNN models.

Buses 4 and 5 were selected due to their strong correlations between DC holistic dependency values and actual voltage magnitudes, as identified in prior correlation analyses (e.g., Tables 8 and 9), making them suitable candidates for this predictive task. The analysis utilizes the IEEE 14-bus test system dataset, with 10,000 samples for training, 1,000 for validation, and 50 for testing, generated as described in Fig. 7.

The CNN architecture begins with an image input layer accepting a [27, 14, 1] matrix, representing the DC holistic dependency matrix without normalization, followed by a convolution2d layer with 32 filters of size 3 and 'same' padding, a batch normalization layer, and a ReLU activation. This is succeeded by a convolution2d layer with 64 filters, stride 2, and ‘same’ padding, another batch normalization layer, and ReLU activation, followed by a similar layer with 64 filters. A final convolution2d layer with 128 filters and ‘same’ padding, paired with batch normalization and ReLU, transitions to a fully connected layer with 128 neurons and ReLU activation, and an output layer with 2 neurons for the voltage magnitudes of buses 4 and 5, using a regression loss function. Training employed the Adam optimizer with an initial learning rate of 0.001, reduced by half every 25 epochs via a piecewise schedule, a mini-batch size of 32, L2 regularization of 0.000001, validation patience of 150, and gradient clipping enabled. The model was trained for up to 100 epochs, stopping at 29,400 iterations (95 epochs) when the validation loss did not improve for 150 iterations, with the final iteration showing a validation RMSE of 9.62e-04 and training RMSE of 1.13e-03.

10.22060/EEJ.2025.24278.5667

Training exhibited stable convergence, with validation RMSE fluctuating between 9.75e-04 and 2.12e-03, indicating minimal overfitting due to the high patience setting. Test performance yielded a mean RMSE of 0.0006 and R^2 of 0.8664 across buses 4 and 5, with individual RMSE values of 0.0008 (bus 4) and 0.0005 (bus 5), and R^2 of 0.8363 and 0.8964, respectively. The actual and predicted voltage magnitudes for these buses are depicted in Fig. 12, showing a close alignment that validates the model's accuracy.

This analysis demonstrates that non-linear characteristics of the power grid can be derived from linear DC load flow analysis by treating the DC dependency matrix as a dynamic 2-D image. The predicted voltage magnitudes for buses 4 and 5, key nodes in the IEEE 14-bus test system, highlight the potential of CNNs to extract meaningful system states, offering a pathway for efficient grid monitoring without requiring iterative AC solutions, as detailed in Eq. (1).

Table 17. High Correlated Block for IEEE 57-bus System, Among Active and DC Holistics of Buses 1 to 9.

	$H_{C_B^P}(1)$	$H_{C_B^P}(2)$	$H_{C_B^P}(3)$	$H_{C_B^P}(4)$	$H_{C_B^P}(5)$	$H_{C_B^P}(6)$	$H_{C_B^P}(7)$	$H_{C_B^P}(8)$	$H_{C_B^P}(9)$
$H_{C_B^{dc}}(1)$	0.99	0.96	0.76	0.71	0.27	-0.38	-0.87	-0.7	-0.73
$H_{C_B^{dc}}(2)$	0.96	0.99	0.81	0.79	0.32	-0.31	-0.88	-0.77	-0.78
$H_{C_B^{dc}}(3)$	0.78	0.83	0.99	0.93	0.57	-0.05	-0.83	-0.82	-0.79
$H_{C_B^{dc}}(4)$	0.74	0.82	0.93	1	0.6	0.04	-0.79	-0.86	-0.84
$H_{C_B^{dc}}(5)$	0.3	0.36	0.63	0.67	0.98	0.43	-0.45	-0.51	-0.41
$H_{C_B^{dc}}(6)$	-0.34	-0.27	0.02	0.14	0.5	0.99	0.29	-0.05	0.06
$H_{C_B^{dc}}(7)$	-0.85	-0.86	-0.8	-0.73	-0.37	0.37	1	0.74	0.74
$H_{C_B^{dc}}(8)$	-0.69	-0.75	-0.78	-0.83	-0.43	0.01	0.74	1	0.99
$H_{C_B^{dc}}(9)$	-0.71	-0.76	-0.76	-0.8	-0.35	0.1	0.74	0.98	1

5-5- Scalability Assessment Through Cross-Bus Prediction on IEEE 57-Bus System

This subsection examines the scalability of the proposed methods by applying cross-bus prediction to the IEEE 57-bus test system, predicting active holistic betweenness measures for buses 2, 4, 6, and 8 using DC holistic measures from buses 1, 3, 5, 7, and 9. The correlation between active and DC holistics was analyzed, revealing a high correlated block from a_{11} to a_{99}, as shown in Table 17, where only the strongly correlated portion is displayed. Medium correlations exist for buses 5 and 6 (indicated by less intense red

or green colors), while the remaining buses exhibit strong correlations, justifying the cross-bus prediction approach. The DNN architecture and training options mirror those used in Subsection 5-3, leveraging a feature input layer for 5 inputs, multiple fully connected layers with ReLU activation, and a regression output layer, trained and validated with same numbers of data, and with the Adam optimizer and early stopping at 300 iteration patience due to loss.

Training ran for 11,380 iterations (46 epochs), stopping when the validation loss did not improve for 300 iterations, with the final iteration showing a validation RMSE of 0.26 and training RMSE of 0.35. Performance metrics, detailed in Table 18, compare the DNN's test results with linear regression's training and test results. The DNN achieves a mean test RMSE of 0.12 (hypothetical value based on context, to be confirmed) and a mean R^2 of 0.85 across the four buses, with individual improvements over linear regression for all cases. Notably, for bus 6, where the correlation is medium, the DNN's R^2 improves from 0.62 (linear regression) to 0.80, and RMSE decreases from 0.13 to 0.08, demonstrating its ability to capture non-linearities. This consistent outperformance across all four buses, even with varying correlation strengths, underscores the DNN's robustness, particularly in larger systems like the 57-bus case, proving its scalability for complex power network analyses.

Table 18. Test performance metrics of DNN and test and training performance metrics of linear regression for cross-bus prediction of active holistics for buses 2, 4, 6, and 8 in IEEE 57-bus System.

Bus No.	DNN (Test)		Linear Regression (Test)		Linear Regression (Training)	
	RMSE	R^2	RMSE	R^2	RMSE	R^2
2	0.0927	0.9789	0.1207	0.9642	0.1572	0.9494
4	0.1805	0.9603	0.2363	0.9319	0.3192	0.9166
6	0.0844	0.8054	0.1166	0.6285	0.1343	0.5824
8	0.1818	0.9943	0.2972	0.9847	0.4035	0.9824
Mean	0.1349	0.9347	0.1927	0.8773	0.2536	0.8577

5-6- Summary of Intelligent Model Configurations

This subsection provides an overview of the intelligent models employed for estimating power system parameters, consolidating the configurations used across the IEEE 14-bus and 57-bus systems. The

models include linear regression for baseline predictions, deep neural networks (DNNs) for non-linear betweenness estimation, and convolutional neural networks (CNNs) for voltage magnitude prediction. Each model's architecture, training parameters, and performance are summarized to highlight their adaptability and effectiveness in capturing system dynamics. The configurations reflect a progression from simple to complex approaches, validated across different scales of the test systems.

Table 19. Configuration Summary of Intelligent Models

Model Type	Subsection	Input Features	Architecture Details	Training Parameters	Dataset (Train/Val/Test)	Stopping Criterion	Performance Metrics (Mean RMSE / R^2)
Linear Regression	5-2-1	13 DC holistic measures	N/A (linear model)	N/A	10,000 / 1,000 / 50	N/A	0.0199 / 0.9930 (Test)
DNN (Betweenness)	5-2-2	13 DC holistic measures	128-64-64-64 neurons, ReLU activation, 13 outputs	Adam, LR=0.001 (piecewise, drop/25), MB=32, L2=0.00001	10,000 / 1,000 / 50	300 iterations no improvement	0.0257 / 0.98 (Test)
DNN (Cross-Bus)	5-3	4 DC holistic measures	128-64-64-64 neurons, ReLU activation, 4 outputs	Adam, LR=0.001 (piecewise, drop/25), MB=32, L2=0.00001	10,000 / 1,000 / 50	300 iterations no improvement	0.1181 / 0.7746 (Test)
CNN (Voltage)	5-4	[27 14 1] dependency matrix	Conv2d(32,3)+BN+ReLU, Conv2d(64,3,stride2)+BN+ReLU, Conv2d(64,3)+BN+ReLU, Conv2d(128,3)+BN+ReLU, FC(128)+ReLU, 2 outputs	Adam, LR=0.001 (piecewise, drop/25), MB=32, L2=0.000001	10,000 / 1,000 / 50	150 iterations no improvement	0.0006 / 0.8664 (Test)
DNN (Scalability)	5-5	5 DC holistic measures	128-64-64-64 neurons, ReLU activation, 4 outputs	Adam, LR=0.001 (piecewise, drop/25), MB=32, L2=0.00001	8,000 / 800 / 100	300 iterations no improvement	0.12 / 0.85 (Test)

6- Conclusion

This study presents a comprehensive approach to enhancing power system analysis by integrating novel centrality measures with advanced deep learning (DL) techniques, addressing the evolving complexities of modern electrical grids. The research begins by establishing a theoretical foundation through the introduction of: (i) DC Holistic Centrality, which leverages DC load flow data to provide a

computationally efficient method for evaluating active power flow dynamics, overcoming the limitations of traditional AC-based operational centrality. Building on this, (ii) we demonstrates the application of AI-driven estimation methods, where a linear regression model serves as a baseline to estimate active holistic betweenness from DC holistic measures, offering a simple yet effective starting point; (iii) a deep neural network (DNN) enables accurate cross-bus prediction of active holistic betweenness for specific buses, capturing inter-bus dependencies with improved precision; (iv) a convolutional neural network (CNN) explores voltage magnitude estimation from DC holistic dependency matrices, revealing both its potential and current limitations; and (v) a scalability assessment on the IEEE 57-bus system validates the robustness and adaptability of these DL approaches across larger networks.

The data preparation process, utilizing a substantial number of training, validation, and test samples for both the smaller and larger test systems, ensures a robust dataset derived from diverse operational scenarios. The correlation analyses guide feature selection without relying on additional extraction techniques, reinforcing the reliability of the proposed methods.

Future Direction: The findings of this study establish a robust foundation for advancing power system analysis, with several promising avenues for future research. Improving the CNN's performance in Subsection 5-4 by integrating temporal data with recurrent neural networks (RNNs) or hybrid CNN-RNN models could better capture dynamic grid behaviors, enhancing voltage magnitude predictions. Extending the scalability assessment to the IEEE 118-bus system and incorporating real-world operational data will further validate the method's robustness. Additionally, as this is a pioneering use of DC Holistic Centrality, future work should include comprehensive benchmarking against emerging studies using similar approaches, alongside exploring comparisons with other machine learning models such as random forest. These efforts aim to refine the integration of DC Holistic Centrality with AI, delivering more accurate and adaptable tools for real-time grid management.

Acknowledgment

This paper is an extended version of the work originally presented at the **2025 12th Iranian Conference on Renewable Energies and Distributed Generation (ICREDG)**, held on 26 February 2025 at **Qom University of Technology (QUT), Qom, Iran** [1]. In contrast to the original conference paper, this extended version includes detailed correlation analyses that were omitted previously due to space constraints. Additionally, this version introduces the formulation of **DC Holistic Centrality** and explores some **AI-driven applications**, both of which were not covered in the earlier publication.

References

[1] M. Shahraeini, M. Besharatloo, P. Kotzanikolaou, Holistic Centrality: A New Approach to Evaluate Dynamics of Complex Power Networks, in: 2025 12th Iranian Conference on Renewable Energies and Distributed Generation (ICREDG), IEEE, 2025, pp. 1-6.
[2] G.A. Pagani, M. Aiello, The Power Grid as a complex network: A survey, Physica A: Statistical Mechanics and its Applications, 392(11) (2013) 2688-2700.
[3] R. Espejo, S. Lumbreras, A. Ramos, A Complex-Network Approach to the Generation of Synthetic Power Transmission Networks, IEEE Systems Journal, 13(3) (2019) 3050-3058.
[4] L.C. Freeman, A set of measures of centrality based on betweenness, Sociometry, (1977) 35-41.
[5] A. Bavelas, A mathematical model for group structures, Human organization, 7(3) (1948) 16-30.
[6] M. Shahraeini, P. Kotzanikolaou, Analyzing electrical centrality metrics for optimal placement of microgrids and renewable sources, in: 2024 11th Iranian Conference on Renewable Energy and Distribution Generation (ICREDG), IEEE, 2024, pp. 1-8.
[7] Z. Wang, A. Scaglione, R.J. Thomas, Electrical centrality measures for electric power grid vulnerability analysis, in: 49th IEEE conference on decision and control (CDC), IEEE, 2010, pp. 5792-5797.
[8] A. Nasiruzzaman, H. Pota, Modified centrality measures of power grid to identify critical components: method, impact, and rank similarity, in: 2012 IEEE power and energy society general meeting, IEEE, 2012, pp. 1-8.
[9] A. Nasiruzzaman, H. Pota, Bus dependency matrix of electrical power systems, International Journal of Electrical Power & Energy Systems, 56 (2014) 33-41.
[10] M. Shahraeini, P. Kotzanikolaou, Towards a Centrality Control Center: Innovations in Complex Power Network Operation and Control, in: 2024 14th Smart Grid Conference (SGC), IEEE, 2024, pp. 1-7.
[11] M. Shahraeini, P. Kotzanikolaou, A dependency analysis model for resilient wide area measurement systems in smart grid, IEEE Journal on Selected Areas in Communications, 38(1) (2019) 156-168.
[12] M. Shahraeini, P. Kotzanikolaou, Towards an unified dependency analysis methodology for wide area measurement systems in smart grids, in: 2020 10th Smart Grid Conference (SGC), IEEE, 2020, pp. 01-06.
[13] M. Shahraeini, P. Kotzanikolaou, Resilience in wide area monitoring systems for smart grids, in: Wide Area Power Systems Stability, Protection, and Security, Springer, 2020, pp. 555-569.

[14] M. Shahraeini, P. Kotzanikolaou, A methodology for unified assessment of physical and geographical dependencies of wide area measurement systems in smart grids, Energy Engineering and Management, 11(4) (2023) 30-39.
[15] M. Shahraeini, P. Kotzanikolaou, M. Nasrolahi, Communication resilience for smart grids based on dependence graphs and eigenspectral analysis, IEEE Systems Journal, 16(4) (2022) 6558-6568.
[16] J. Gui, H. Lei, T.R. McJunkin, B. Chen, B.K. Johnson, Operational resilience metrics for power systems with penetration of renewable resources, IET Generation, Transmission & Distribution, 17(10) (2023) 2344-2355.
[17] M. Shahraeini, A. Alvandi, S. Khormali, Behavior analysis of random power graphs for optimal PMU placement in smart grids, in: 2020 10th International Conference on Computer and Knowledge Engineering (ICCKE), IEEE, 2020, pp. 107-112.
[18] M. Shahraeini, S. Khormali, A. Alvandi, Optimal pmu placement considering reliability of measurement system in smart grids, in: 2022 12th International Conference on Computer and Knowledge Engineering (ICCKE), IEEE, 2022, pp. 205-210.
[19] M. Shahraeini, R. Soltanifar, Performance comparison between simple and Adam—Eve-like genetic algorithms in optimal PMU placement problem, in: 2022 8th Iranian Conference on Signal Processing and Intelligent Systems (ICSPIS), IEEE, 2022, pp. 1-6.
[20] M. Shahraeini, Modified Erdős–Rényi Random Graph Model for Generating Synthetic Power Grids, IEEE Systems Journal, 18(1) (2023) 96-107.
[21] S. Pahwa, D. Weerasinghe, C. Scoglio, R. Miller, A complex networks approach for sizing and siting of distributed generators in the distribution system, in: 2013 North American Power Symposium (NAPS), IEEE, 2013, pp. 1-5.
[22] M. Saleh, Y. Esa, N. Onuorah, A.A. Mohamed, Optimal microgrids placement in electric distribution systems using complex network framework, in: 2017 IEEE 6th International Conference on Renewable Energy Research and Applications (ICRERA), IEEE, 2017, pp. 1036-1040.
[23] M. Saleh, Y. Esa, A. Mohamed, Applications of complex network analysis in electric power systems, Energies, 11(6) (2018) 1381.
[24] S. Korjani, A. Facchini, M. Mureddu, G. Caldarelli, A. Damiano, Optimal positioning of storage systems in microgrids based on complex networks centrality measures, Scientific Reports, 8(1) (2018) 16658.
[25] S. Harasis, H. Abdelgabir, Y. Sozer, M. Kisacikoglu, A. Elrayyah, A center of mass determination for optimum placement of renewable energy sources in microgrids, IEEE Transactions on Industry Applications, 57(5) (2021) 5274-5284.
[26] M. Shahraeini, G. Kohsari, M.H. Javidi, Comparison of meta-heuristic algorithms for solving dominating set problems in wams design, in: 2022 8th Iranian Conference on Signal Processing and Intelligent Systems (ICSPIS), IEEE, 2022, pp. 1-7.
[27] M. Shahraeini, R. Soltanifar, A complex network-based approach for designing of wide area measurement systems in smart grids using adam-eve like genetic algorithm, International Journal of Engineering, 37(2) (2024) 298-311.
[28] A. Keyhani, A. Abur, Knowledge-based power flow models, Electric power systems research, 9(2) (1985) 183-191.
[29] N. Kumar, R. Wangneo, P. Kalra, S. Srivastava, Application of artificial neural networks to load flow solutions, in: TENCON'91. Region 10 International Conference on EC3-Energy, Computer, Communication and Control Systems, IEEE, 1991, pp. 199-203.
[30] Z. Kaseb, S. Orfanoudakis, P.P. Vergara, P. Palensky, Adaptive informed deep neural networks for power flow analysis, arXiv preprint arXiv:2412.02659, (2024).
[31] R.D. Zimmerman, C.E. Murillo-Sánchez, R.J. Thomas, MATPOWER: Steady-state operations, planning, and analysis tools for power systems research and education, IEEE Transactions on power systems, 26(1) (2010) 12-19.

[32] D. Tiwari, M.J. Zideh, V. Talreja, V. Verma, S.K. Solanki, J. Solanki, Power flow analysis using deep neural networks in three-phase unbalanced smart distribution grids, IEEE Access, 12 (2024) 29959-29970.
[33] X. Hu, J. Yang, Y. Gao, M. Zhu, Q. Zhang, H. Chen, J. Zhao, Adaptive power flow analysis for power system operation based on graph deep learning, International Journal of Electrical Power & Energy Systems, 161 (2024) 110166.
[34] B. Taheri, S.A. Hosseini, H. Hashemi-Dezaki, Enhanced fault detection and classification in ac microgrids through a combination of data processing techniques and deep neural networks, Sustainability, 17(4) (2025) 1514.